博士論文

Collective dynamics of self-driven particles with attachment and detachment

(吸脱着機構を持つ自己駆動粒子系の集団動力学)

一木　信吾

Contents

List of Figures

List of Tables

Chapter 1

Introduction

1.1 Preface

It is possible to capture many phenomena in nature and society as macroscopic behaviors built up by collective behavior of microscopic particles. Among them, crowd dynamics, traffic flow, and others belong to the systems of self-driven particles, and phenomena showed by dynamics of these systems offer important issues to today's science. Systems of self-driven particles are groups of particles which have their own intention and can move voluntarily [1–4]. In other words, the systems can be considered a collection of particles moving according to a rule which does not satisfy the basic principles of mechanics (law of inertia, law of motion, and law of action and reaction) [2, 3].

In traditional physics, research has been conducted on what satisfy basic principles of mechanics as the main subjects [2]. For example, in the case of properties of water which is a substance consisting of many molecules, detailed theories are formed from empirical facts and experimental results, and they have built up one of the largest field of physics as fluid dynamics [5]. On the other hand, for the case of the flow of self-driven particles such as crowd and traffic flow, the research history on them is shorter than traditional physical fields and the common basic law has not been found fundamentally so far [2, 3]. Therefore, the precise formulation is difficult and the studies have been advanced by qualitative methods such as simple modelings of the dynamics in the individual phenomenon [2, 3].

Moreover, most of the self-driven-particle systems are the non-equilibrium systems in which particles can inflow and outflow freely. These are always in states far from the equilibrium state in which the physical quantity is bal-

anced. Whereas thermodynamics and statistical mechanics have been built as an established ground in the equilibrium state of matter, the science dealing with the non-equilibrium system has not been systematized sufficiently yet [6, 7]. Therefore, it is one of the significant goals of modern science to find the basic law in the non-equilibrium system for better comprehending and controlling the nature and the social phenomena.

Because of the points above, it is highly important to understand the phenomena mathematically through the viewpoint of the collective dynamics in which a large number of self-driven particles interact with each other. Moreover, filing various systems of self-driven-particles and analyzing their behavior qualitatively are considered to be widely contributory to finding the basic laws of them and building new physical fields.

In this thesis we focus on the systems of self-driven particles in which the conservation of the number of particles is not kept constant because particles attach and detach at any point. Various relevant phenomena are observed because of the interaction of particles coming in to and going out of the system. Therefore, it is greatly interesting to study the collective behavior of particles from the point of view of the mechanism of attachment and detachment. We will call the system as the "system of self-driven particles with attachment and detachment" in this thesis. For these systems, we study in order to understand the universal principle and the structure in cross-cutting. Therefore, considering the mechanism of attachment and detachment, we aim to constructing the mathematical models which enable us a more wide generalization. In addition, we mathematically analyze the effect that mechanism of attachment and detachment cause to the systems by using the constructed models. In the results, we reveal some phenomena caused by the mechanism of attachment and detachment more in detailed.

1.2 Actual systems of self-driven particles with attachment and detachment

We will show here three concrete examples about systems of self-driven particles with attachment and detachment which are the objective of this thesis. In this thesis, our main aim is to understand the phenomena and the structure seen in the concrete examples we introduce here.

First of all, we give a transport phenomenon in cells as one of the representative examples. Our explanations have about the transport phenomenon in the cell is based on references [2, 8–11]. Cells have a cytoskeleton to ar-

range orderly various structural components, change the form, and move. The cytoskeleton is a network structure composed of protein filaments. In particular, the protein filament called a microtubule plays a role of keeping order in a cell. Structural components of cells are transported by motor proteins along this transport network in the cells.

The motor protein in axon of neuron has two types: a type of kinesins and a type of dyneins. The kinesin moves to the plus direction, on the other hand the dynein moves to the minus direction on the microtubule (Fig. 1.1 [2,8–11]). They have a motion due to the interaction of each other that is determined by the biochemical cycle. Thus, we consider these motor proteins as self-driven particles.

Moreover, the motor protein does not move only in one microtubule, but also transfers to other microtubules one after another [2]. Therefore, the transport mechanism like this can be considered to be a system of self-driven particles with attachment and detachment.

Studies which capture transport phenomena in the body as in the example above have been actively conducted [10]. It is important for biology to understand the transportation mechanism of chemical substances in the body.

In Chap. 2, we review a simple mathematical model which was studied in biological physics based on Parmeggiani *et al.* [12] and Evans *et al.* [13]. The mathematical model we introduce in Chap. 2 is the basis of the study in this thesis.

Next, we give a traffic flow with lane changing as another example (Fig. 1.2). Cars go forward considering the distance between the front car using the accelerator and the brakes. From this fact, we can regard a car as a self-driven particle because it is moved voluntarily by a person with intention.

In addition, when it becomes crowded in a traffic lane on a roadway with multiple lanes in each direction, a car on this lane is supposed to change out to another lane. On the other hand, a car is supposed to change to the lane from other crowded lane. That is to say, we can consider the lane changing to be the mechanism of attachment and detachment of particles.

Recently, studies about the traffic flow focusing on lane changing have been carried out [14]. It is important for modern society to analyze the influence of lane changing on the traffic flow in the meaning of understanding mechanism of traffic jam. Furthermore, results from these studies, can be considered to be useful for improvement of the traffic jam.

In Chap. 3, we propose a mathematical model considering a basic characteristic of the traffic flow with lane changing and show its analytical results.

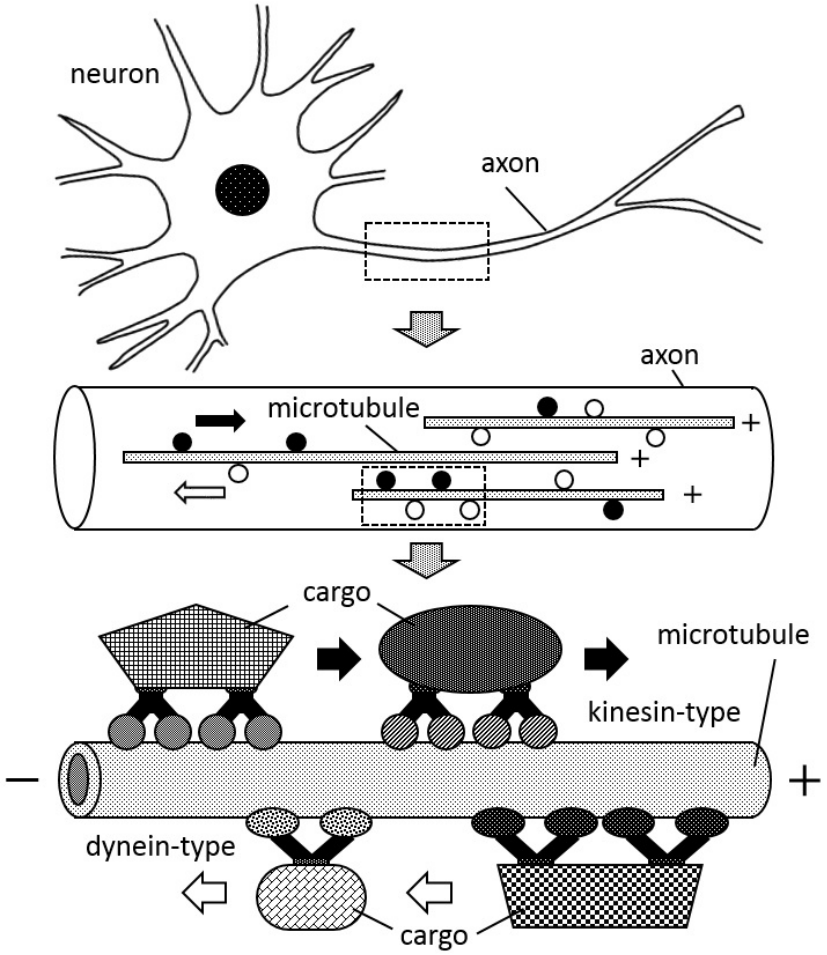

Figure 1.1: Conceptual diagram of the motor protein in an axon

In addition, in Chap. 4, we introduce the result on about a mathematical model which expands the model proposed in Chap. 3.

Finally, we give a trading mechanism in financial instruments exchanges as the other example, which has distinctive features from the other examples. Many financial instruments exchanges, use the electronic board called order book on which the order status of sellers and buyers of a certain product is recorded (Fig. 1.3) [15–17]. This trading mechanism in which sellers and buyers present the price each other is called continuous double auction system [16, 18].

In the order book, the order or its cancel is conducted by decision of

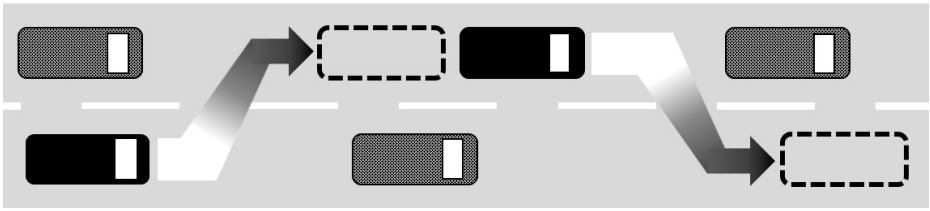

Figure 1.2: Conceptual diagram of the traffic flow with lane changing

the trader. Furthermore, the price changes according to the trading rule provided in the exchange. In addition, once the price changes, the orders on the order book are moved by the traders depending on this change. From these above, the movement of the order in the order book is considered to be the system of self-driven particles with attachment and detachment. On the other hand, it is different from the systems of vehicular traffic and motor proteins in the sense that some orders (particles) can exist in the same price. This system seen at the order book has been interested as a non-equilibrium system in the field such as econophysics [19, 20].

In Chap. 5, we consider the actual complex system seen in the order book shown in Fig. 1.3 from the concrete point of view. By considering the concrete complex system, we can deepen our understanding about the importance of study on the mathematical model on the viewpoint of the mechanism of attachment and detachment introduced in Chap. 3 and 4.

In this thesis, against the background of the actual systems of self-driven particles with attachment and detachment mentioned as examples above, we propose and analyze some mathematical models for the purpose of understanding on these basic dynamics.

1.3 Asymmetric simple exclusion process

We will explain here the summary of the asymmetric simple exclusion process (ASEP), which is a basis of the mathematical model we introduce in this thesis.

The ASEP is a stochastic process on non-equilibrium statistical dynamics in which many particles diffuse under interaction for excluded volume on a

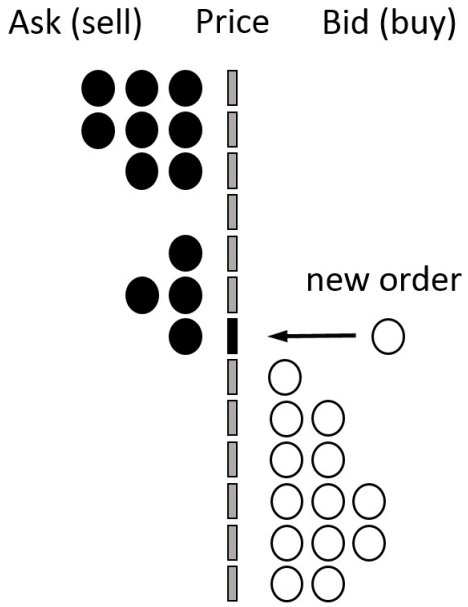

Figure 1.3: Conceptual diagram of the order book in financial instruments exchanges

lattice [21]. The ASEP is composed of a one-dimensional lattice consisting of L sites and particles existing on the lattice. Only two patterns of situations possibly exist in each site i $(1 \leq i \leq L)$: there is a particle $(\tau_i = 1)$ or there is no particle $(\tau_i = 0)$. In other words, there are 2^L patterns of configurations of particles on the lattice in total. Then, each particle performs random walk asymmetrically. However, a particle cannot move if other particles exist in target sites because only one particle can exist in each site.

In the ASEP, there are two patterns of boundary conditions as we show in Fig. 1.4: a periodic boundary and an open boundaries.

In the case of the periodic boundary, we consider the initial condition that some particles are in the periodic lattice. Then, these particles hop to a certain direction at the rate p and to the opposite direction at the rate q $(p \neq q)$. The number of the particles in the initial condition is kept constant because any particle does not go out from the lattice.

On the other hand, in the case of the open boundaries, particles are injected at the rate α and removed at the γ from one end of the lattice. In addition, particles are removed at the rate β and injected at the rate δ from the other end. Since particles come in and go out from both ends of the

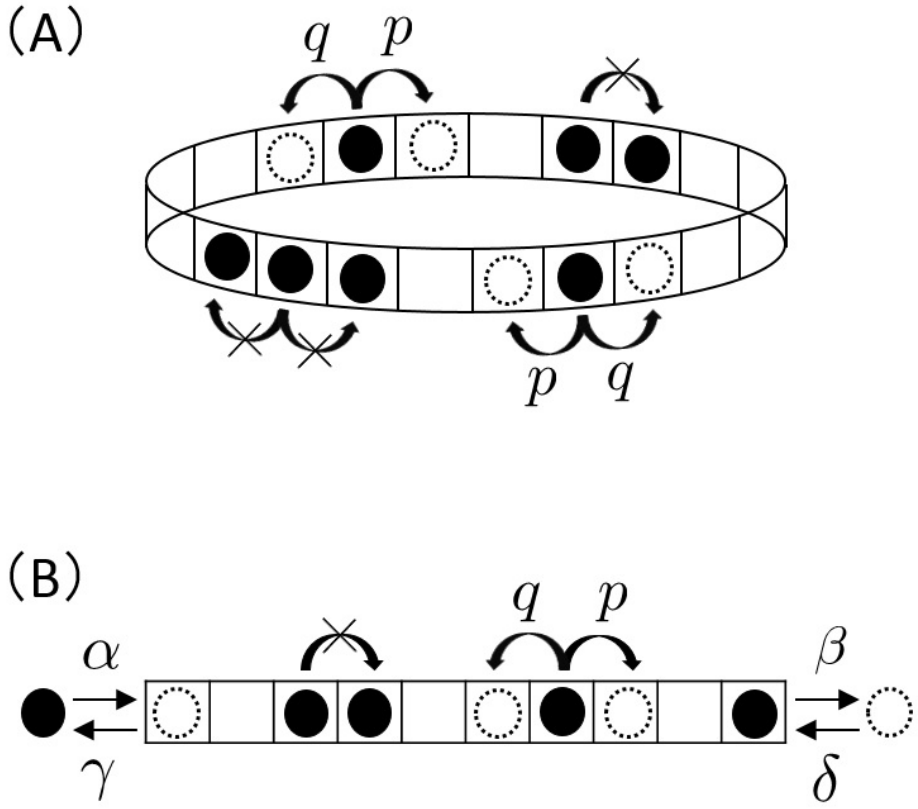

Figure 1.4: Schematic diagram of the ASEP with (A) a periodic boundary and (B) an open boundaries.

lattice, the number of the particles on the lattice is not kept. The move of particle at the part of bulk is the same as the case of the periodic boundary.

The ASEP was first introduced in 1986 as the model of ribosome which moves on m-RNA [22]. Since the steady state on an open boundaries was exactly solved by the method called Matrix Products Ansatz by Derrida *et al.* in 1993, it has become widely known [23]. Since then, various studies on the ASEP have been carried out as an attractive model to study the non-equilibrium systems [24–26].

Especially in the case of $q = \gamma = \delta = 0$, it is called totally asymmetric simple exclusion process (TASEP). In the TASEP with an open boundaries, it is also known from previous studies that the steady state of the system is greatly affected by the inflow rate α and the outflow rate β at the boundaries [26–28]. In particular, there are three different phases (the low-density phase, the high-density phase, and the maximal current phase) depending on the value of the rates of inflow and outflow at the boundaries. Furthermore, in the phase diagram, there is a domain of inflow and outflow rates (a coexistence line) where the low-density domain and the high-density domain coexist on the density profile. On the coexistence line, a point of discontinuity called domain wall (DW) is known to perform random walk in the density profile [24, 26]. A DW is equivalent to a shock wave in fluid dynamics. In recent years, the TASEP has been extensively used to study the systems the flow of self-driven particles such as traffic flow and queue of people [4, 29–31].

In addition, mathematical models where a mechanism of attachment and detachment is built in TASEP has been actively studied in recent years. This model is called the totally asymmetric simple exclusion process with Langmuir kinetics (TASEP-LK). Langmuir kinetics is the mechanism of attachment and detachment of the particles at the bulk of a lattice. In Chap. 2, we explain the original TASEP-LK in detail. In this thesis, we generalize this model, and study the dynamical structure of the system of self-driven particles with attachment and detachment.

1.4 Organization of this thesis

The organization of this thesis is as follows.

In Chap. 2, we summarize the previous studies which are related to the mathematical models we propose in this thesis. In particular, we explain the original TASEP-LK with a periodic boundary and an open boundaries, respectively. These models provide a basis for our models. For the first, in

the original TASEP-LK with a periodic boundary, we account for deriving the exact stationary distribution based on the result of Ezaki and Nishinari [32]. In the second, in the original TASEP-LK with an open boundaries, we explain the analyzing method with a mean-field approximation based on the result of Parmeggiani *et al.* [12] and Evans *et al.* [13].

In Chap. 3, we propose the TASEP on a periodic lattice with LK depending on the state of the forward neighboring site [33]. We mathematically analyze the steady state and relaxation dynamics using a mean-field approximation. We show that the structure of dynamics for the model is captured accurately by performing simulations for the model.

In Chap. 4, we propose the TASEP on an open lattice with LK depending on the state of the forward and backward neighboring sites [34]. In particular, we analyze the case in which the rate of attachment and detachment are equivalent in detail. As with Chap. 3, we mathematically analyze the steady state using a mean-field approximation. We prove that the situation of the steady state is captured mathematically through comparison between the analytical result and the simulation result.

In Chap. 5, we take up actual system of self-driven particles with attachment and detachment which is our object in this thesis. Then, we capture the phenomena caused by the mechanism of attachment and detachment from a more concrete point of view. In particular, as an actual complex system, we pick up a trading mechanism in the financial instruments exchange. We propose the simulating models reproducing the basic properties of this trading mechanism, and examine the effect of the mechanism of attachment and detachment on the system [35, 36].

Finally, Chap. 6 is devoted to the conclusion in this thesis.

Chapter 2

Totally asymmetric simple exclusion process with Langmuir kinetics

2.1 Preface

We will review here the TASEP with a mechanism of attachment and detachment called Langmuir kinetics (LK) and its applications [4]. The basic mechanism of the model is explained as follows: a particle attaches at a certain rate when a selected site on the lattice is empty, whereas a particle detaches at a certain rate when a target site is occupied. The TASEP with a mechanism of attachment and detachment is called "TASEP-LK" in this thesis. Figure 2.1 shows a schematic of the original TASEP-LK with an open boundaries, where ω_{A}, ω_{D}, and p denote the attachment, detachment, and hopping rates respectively. The rates of the inflow and outflow at the boundaries are denoted by α and β, respectively.

Recently, there have been many studies on the TASEP-LK and its applications [4]. For the original TASEP-LK with an open boundaries, Parmeggiani *et al*. analyzed the case where the attachment rate ω_{A} was three times as high as the detachment rate ω_{D} ($K = \omega_{\mathrm{A}}/\omega_{\mathrm{D}} = 3$) by applying a mean field approximation and performing Monte Carlo simulations [12]. In their study, it was found that the results from the numerical calculation and simulations agreed well if the number of lattice sites was large. Furthermore, Evans *et al*. developed a detailed argument by using a mean-field approximation for the general rates of the attachment and detachment [13]. After that, Parmeggiani *et al*. have shown the more detailed results on TASEP-

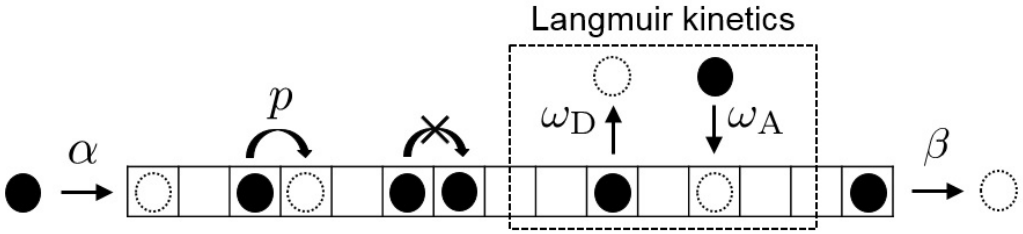

Figure 2.1: Schematic diagram of the original TASEP-LK with an open boundaries.

LK in [37]. In addition, the dynamics of a kink, which is an interesting phenomenon in the TASEP-LK, was studied in [38].

After that, many models which expanded the original TASEP-LK have been proposed in the context of biophysics. As a representative applied research, we can give the study analyzing the transport dynamics on single-headed kinesin motors by Nishinari *et al.* [10]. In their study, the model in which some different types of particles moving variously were considered was proposed in order to reproduce the complex chemical reaction. On the other hand, from the standpoint of the basic research, strict analysis about ASEP-LK of the multi-species particles was conducted [39]. In addition, the model with hopping rates depending on the state of the neighboring sites has also been studied [40]. This is the model where LK is added to the Katz-Lebowitz-Spohn (KLS) model [41, 42]. Moreover, the model with LK depending on the state of the neighboring sites has been proposed as well [43]. This model is closely related to our model introduced in this thesis. In Chap. 4, we introduce the extended model about the case in which the attachment rate and the detachment rate have equal condition in the model introduced in their paper. Additionally other distinctive TASEP-LK models in the presence of randomly distributed inhomogeneities [44] and in a growing lattice were proposed [45].

In recent years, the TASEP-LK has been actively studied not only with one lane but also with multiple lane [46]. In the multi-lane models, it is set that a single lane of the TASEP-LK is arranged side by side, then particles come and go between the mutual lanes. These models can be considered that they are developed for the lane changing in the traffic flow.

Furthermore, the TASEP-LK have been applied to the networks as models for complex transport phenomena [47, 48]. These are the models where multiple single-lane TASEP-LK are connected to the network form. Neri *et*

al. have researched how the transport phenomenon receives influence by the form of the network [47, 48].

Besides these models, a similar model without translational motion of particles was proposed in a study of granular materials [49]. This is the model on the dynamics of falling of granular particles, and we can say that in such a model only LK is implemented.

In the next section and beyond, we introduce the original TASEP-LK based on some previous studies as the basis for our models studied in this thesis. For the first, we show the exact solution in the steady state with regard to the original TASEP-LK with a periodic boundary in Sec. 2.2 based on Ezaki and Nishinari [32]. Furthermore, we explain the original TASEP-LK with an open boundaries in Sec. 2.3 according to the results of Parmeggiani *et al.* [12] and Evans *et al.* [13]. In Chaps. 3 and 4, we show the analysis result on the model we propose by use of the analyzing method explained in Sec. 2.3.

2.2 Periodic boundary

We fully explain here the derivation of an exact stationary distribution for the original TASEP-LK with a periodic boundary based on Ezaki and Nishinari [32].

2.2.1 Model

Let us consider a one-dimensional periodic lattice consisting of L sites. Each site can either be empty ($\tau_i = 0$) or occupied with a single particle ($\tau_i = 1$). Here, $\tau_i \in \{0, 1\}$ denotes the occupation of site i. We assume that a particle can move to the site in front at rate $p = 1$ if it is vacant. Additionally, the attachment rate and the detachment rate are ω_{A} and ω_{D}, respectively. Figure 2.2 shows a schematic of the original TASEP-LK with a periodic boundary.

2.2.2 Exact stationary distribution

We present an exact probability distribution for the configuration particles in the steady state.

The stationary probability distribution P can be written in the following

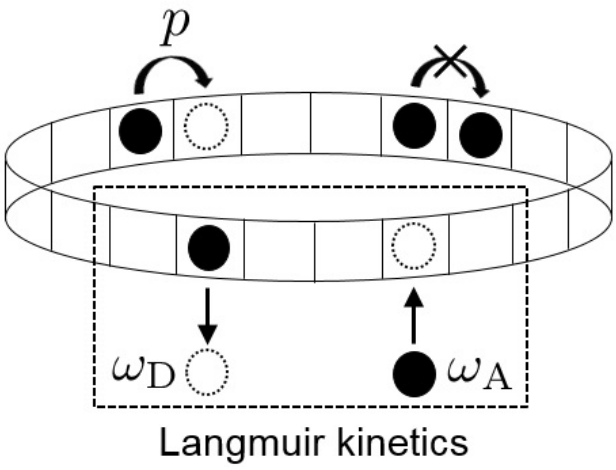

Figure 2.2: Schematic diagram of the original TASEP-LK with a periodic boundary.

form:

$$P(\mathcal{C}) = \Xi_L^{-1}\Phi(N), \tag{2.1}$$

where

$$\Phi(N) = \left(\frac{\omega_{\mathrm{A}}}{\omega_{\mathrm{D}}}\right)^N, \tag{2.2}$$

and

$$\Xi_L = \sum_{N=0}^{L}\left(\frac{\omega_{\mathrm{A}}}{\omega_{\mathrm{D}}}\right)^N\binom{L}{N} = \left(1+\frac{\omega_{\mathrm{A}}}{\omega_{\mathrm{D}}}\right)^L, \tag{2.3}$$

where $\mathcal{C}$ denotes the configurations $\{\tau_1 \cdots \tau_L\}$. The integer N is the number of particles for a given configuration, i.e.

$$N = \sum_{i=1}^{L}\tau_i. \tag{2.4}$$

Moreover, the expectation value of the quantity ρ at a site is calculated as:

$$\rho = \Xi_L^{-1}\sum_{N=1}^{L}\left(\frac{\omega_{\mathrm{A}}}{\omega_{\mathrm{D}}}\right)^N\binom{L-1}{N-1} = \frac{\omega_{\mathrm{A}}/\omega_{\mathrm{D}}}{1+\omega_{\mathrm{A}}/\omega_{\mathrm{D}}}. \tag{2.5}$$

Proof 2.2.1 We prove that (2.1) gives an exact solution of the system. Specifically, it is sufficient to confirm that (2.1) satisfies the following master equation [26]:

$$0 = \frac{\mathrm{d}}{\mathrm{d}t}P(\mathcal{C}) = \sum_{\substack{\tilde{\mathcal{C}} \\ \tilde{\mathcal{C}}\neq\mathcal{C}}} \Big[P(\tilde{\mathcal{C}})W(\tilde{\mathcal{C}} \to \mathcal{C}) - P(\mathcal{C})W(\mathcal{C} \to \tilde{\mathcal{C}}) \Big]. \tag{2.6}$$

where $W(\mathcal{C} \to \tilde{\mathcal{C}})$ denotes the transition rate from configuration $\mathcal{C}$ to $\tilde{\mathcal{C}}$. In the case of the original TASEP-LK, this is explicitly written as:

$$\begin{aligned}
\frac{\mathrm{d}}{\mathrm{d}t}P(\mathcal{C}) = &\sum_{i=1}^{L}(1-\tau_{i-1})\tau_i P(\tau_1 \cdots \tau_{i-2}10\tau_{i+1}\cdots\tau_L) \\
&- \sum_{i=1}^{L}\tau_i(1-\tau_{i+1})P(\mathcal{C}) \\
&+ \sum_{i=1}^{L}\tau_i P(\tau_1 \cdots \tau_{i-1}0\tau_{i+1}\cdots\tau_L)\omega_{\mathrm{A}} - \sum_{i=1}^{L}(1-\tau_i)P(\mathcal{C})\omega_{\mathrm{A}} \\
&+ \sum_{i=1}^{L}(1-\tau_i)P(\tau_1 \cdots \tau_{i-1}1\tau_{i+1}\cdots\tau_L)\omega_{\mathrm{D}} - \sum_{i=1}^{L}\tau_i P(\mathcal{C})\omega_{\mathrm{D}},
\end{aligned} \tag{2.7}$$

where $\tau_0 = \tau_L$ and $\tau_{L+1} = \tau_1$. The first term on the right-hand side of (2.7) is rewritten the following form due to the translational invariance of the model:

$$\begin{aligned}
&\sum_{i=1}^{L}(1-\tau_{i-1})\tau_i P(\tau_1 \cdots \tau_{i-2}10\tau_{i+1}\cdots\tau_L) \\
&\qquad = \sum_{i=1}^{L}(1-\tau_i)\tau_{i+1}P(\tau_1 \cdots \tau_{i-1}10\tau_{i+2}\cdots\tau_L).
\end{aligned} \tag{2.8}$$

The hopping terms are calculated as:

$$\begin{aligned}
&\sum_{i=1}^{L}(1-\tau_i)\tau_{i+1}P(\tau_1\cdots\tau_{i-1}10\tau_{i+2}\cdots\tau_L)-\sum_{i=1}^{L}\tau_i(1-\tau_{i+1})P(\mathcal{C})\\
&\qquad=\sum_{i=1}^{L}(\tau_{i+1}-\tau_i)P(\tau_1\cdots\tau_{i-1}10\tau_{i+2}\cdots\tau_L)\\
&\qquad=\sum_{i=1}^{L}(\tau_{i+1}-\tau_i)\Big(\frac{\omega_{\mathrm{A}}}{\omega_{\mathrm{D}}}\Big)^{N},\\
&\qquad=\Big(\frac{\omega_{\mathrm{A}}}{\omega_{\mathrm{D}}}\Big)^{N}\Big[\sum_{i=1}^{L}\tau_{i+1}-\sum_{i=1}^{L}\tau_i\Big]=0. \qquad (2.9)
\end{aligned}$$

Next, the Langmuir terms are considered as follows:

$$\begin{aligned}
&\sum_{i=1}^{L}\tau_iP(\tau_1\cdots\tau_{i-1}0\tau_{i+1}\cdots\tau_L)\omega_{\mathrm{A}}-\sum_{i=1}^{L}\tau_iP(\mathcal{C})\omega_{\mathrm{D}}\\
&\quad+\sum_{i=1}^{L}(1-\tau_i)P(\tau_1\cdots\tau_{i-1}1\tau_{i+1}\cdots\tau_L)\omega_{\mathrm{D}}-\sum_{i=1}^{L}(1-\tau_i)P(\mathcal{C})\omega_{\mathrm{A}}\\
&\qquad=\sum_{i=1}^{L}\tau_i\Big(\frac{\omega_{\mathrm{A}}}{\omega_{\mathrm{D}}}\Big)^{N-1}\omega_{\mathrm{A}}-\sum_{i=1}^{L}\tau_i\Big(\frac{\omega_{\mathrm{A}}}{\omega_{\mathrm{D}}}\Big)^{N}\omega_{\mathrm{D}}\\
&\qquad\quad+\sum_{i=1}^{L}(1-\tau_i)\Big(\frac{\omega_{\mathrm{A}}}{\omega_{\mathrm{D}}}\Big)^{N+1}\omega_{\mathrm{D}}-\sum_{i=1}^{L}(1-\tau_i)\Big(\frac{\omega_{\mathrm{A}}}{\omega_{\mathrm{D}}}\Big)^{N}\omega_{\mathrm{A}}\\
&\qquad=0. \qquad (2.10)
\end{aligned}$$

Therefore, (2.1) was shown to be the exact stationary distribution from (2.9) and (2.10).

□

2.3 Open boundary

We explain herein a density profile in the steady state for the original TASEP-LK with an open boundaries based on the results obtained by Parmeggiani *et al.* [12] and Evans *et al.* [13].

2.3.1 Model

Let us consider a one-dimensional periodic lattice consisting of L ($L \geq 3$) sites. Each site can either be empty ($\tau_i = 0$) or occupied with a single particle ($\tau_i = 1$). Here, $\tau_i \in \{0, 1\}$ denotes the occupation of site i. We assume that a particle can move to the site in front at rate $p = 1$ if it is vacant. Then, a particle is injected at the rate α from the other end of the lattice, and is removed at the rate β from one end of lattice. Additionally, the attachment rate and the detachment rate is ω_{A} and ω_{D}, respectively.

2.3.2 Analysis on model

We obtain the relational expressions with regard to the density profile by using a mean-field approximation in this section.

2.3.2.1 Mean-field approximation and hydrodynamic limit

We derive herein a partial differential equation satisfied by the density profile.

At site i ($0 < i < L$), the following equation can be expressed from the master equation:

$$\frac{\mathrm{d}\langle\tau_i\rangle}{\mathrm{d}t} = \langle\tau_{i-1}(1-\tau_i)\rangle - \langle\tau_i(1-\tau_{i+1})\rangle + \ \omega_{\mathrm{A}}\langle 1-\tau_i\rangle - \omega_{\mathrm{D}}\langle\tau_i\rangle, \tag{2.11}$$

where $\langle\cdot\rangle$ denotes the expectation value of the quantity. In addition, the equation for the boundary is as follows:

$$\frac{\mathrm{d}\langle\tau_i\rangle}{\mathrm{d}t} = \alpha\langle 1-\tau_1\rangle - \langle\tau_1(1-\tau_2)\rangle - \omega_{\mathrm{D}}\langle\tau_1\rangle, \tag{2.12}$$

$$\frac{\mathrm{d}\langle\tau_L\rangle}{\mathrm{d}t} = \langle\tau_{L-1}(1-\tau_L)\rangle - \beta\langle\tau_L\rangle + \omega_{\mathrm{A}}\langle 1-\tau_L\rangle. \tag{2.13}$$

Then, we perform a mean-field approximation in (2.11). In other words, we factor the correlation functions as follow [50]:

$$\langle\tau_i\tau_{i+1}\rangle \approx \langle\tau_i\rangle\langle\tau_{i+1}\rangle. \tag{2.14}$$

Moreover, we perform the hydrodynamic limit. The expectation value $\langle\tau_{i\pm1}\rangle$ is expanded as:

$$\langle\tau_{i\pm1}\rangle = \rho(x) \pm \frac{1}{L}\frac{\partial\rho}{\partial x} + \frac{1}{2}\frac{1}{L^2}\frac{\partial^2\rho}{\partial x^2} + \mathcal{O}\Big(\frac{1}{L^3}\Big). \tag{2.15}$$

Substituting the first and second terms of this into (2.11), we obtain the following partial differential equation by setting $t = \bar{t}L$ and $L \to \infty$:

$$\frac{\partial \rho}{\partial \bar{t}} + (1-2\rho)\frac{\partial \rho}{\partial x} = \Omega_{\mathrm{A}} - (\Omega_{\mathrm{A}} + \Omega_{\mathrm{D}})\rho, \tag{2.16}$$

where $\Omega_{\mathrm{A}} = \omega_{\mathrm{A}} L$ and $\Omega_{\mathrm{D}} = \omega_{\mathrm{D}} L$ are kept finite. In addition, the boundary conditions become approximately $\rho(0) = \alpha$ and $\rho(1) = 1 - \beta$ from (2.12) and (2.13).

2.3.2.2 Steady-state solution

We construct a solution satisfied by the density profile in the steady state from the partial differential equation (2.16).

In the steady state, the density does not change with respect to time. Thus, we replace the $\partial\rho/\partial\bar{t}$ in (2.16) with 0 and construct a solution by integrating the following differential equation for the density:

$$\frac{\mathrm{d}\rho}{\mathrm{d}x} = \frac{\Omega_{\mathrm{A}} - (\Omega_{\mathrm{A}} + \Omega_{\mathrm{D}})\rho}{(1-2\rho)}. \tag{2.17}$$

Next, we obtain from (2.17) the solutions satisfied by the boundary conditions $\rho(0) = \alpha$ and $\rho(1) = 1 - \beta$, respectively.

Firstly, when (2.17) is integrated for the density ρ from the left end, the following equation is obtained:

$$\begin{aligned} x &= \int_{\alpha}^{\rho_{\mathrm{L}(x)}} \frac{(1-2\rho)}{\Omega_{\mathrm{A}} - (\Omega_{\mathrm{A}} + \Omega_{\mathrm{D}})\rho} \mathrm{d}\rho \\ &= \frac{2(\rho_{\mathrm{L}} - \alpha)}{\Omega_{\mathrm{A}} + \Omega_{\mathrm{D}}} + \frac{\Omega_{\mathrm{A}} - \Omega_{\mathrm{D}}}{(\Omega_{\mathrm{A}} + \Omega_{\mathrm{D}})^2} \log\Big| \frac{\Omega_{\mathrm{A}} - (\Omega_{\mathrm{A}} + \Omega_{\mathrm{D}})\rho_{\mathrm{L}}}{\Omega_{\mathrm{A}} - (\Omega_{\mathrm{A}} + \Omega_{\mathrm{D}})\alpha} \Big|. \end{aligned} \tag{2.18}$$

Further, when (2.17) is integrated for the density ρ from the right end, the following equation is obtained:

$$\begin{aligned} 1 - x &= \int_{\rho_{\mathrm{R}(x)}}^{1-\beta} \frac{(1-2\rho)}{\Omega_{\mathrm{A}} - (\Omega_{\mathrm{A}} + \Omega_{\mathrm{D}})\rho} \mathrm{d}\rho \\ &= \frac{2(1-\beta-\rho_{\mathrm{R}})}{\Omega_{\mathrm{A}} + \Omega_{\mathrm{D}}} \\ &\quad + \frac{\Omega_{\mathrm{A}} - \Omega_{\mathrm{D}}}{(\Omega_{\mathrm{A}} + \Omega_{\mathrm{D}})^2} \log\Big| \frac{\Omega_{\mathrm{A}} - (\Omega_{\mathrm{A}} + \Omega_{\mathrm{D}})(1-\beta)}{\Omega_{\mathrm{A}} - (\Omega_{\mathrm{A}} + \Omega_{\mathrm{D}})\rho_{\mathrm{R}}} \Big|. \end{aligned} \tag{2.19}$$

Next, we consider the discontinuity (domain wall; DW) observed in the density profile. From the balance of mass current, the velocity of the DW, v_{DW}, is expressed as follows:

$$v_{\mathrm{DW}} = \frac{\rho_{\mathrm{R}}(1-\rho_{\mathrm{R}}) - \rho_{\mathrm{L}}(1-\rho_{\mathrm{L}})}{\rho_{\mathrm{R}} - \rho_{\mathrm{L}}} = 1 - \rho_{\mathrm{L}} - \rho_{\mathrm{R}}. \tag{2.20}$$

In the original TASEP-LK, it is known from the simulations that the DW is stable in the steady state. Therefore, we consider the situation with $v_{\mathrm{DW}} = 0$ in (2.20). The relationship between the densities of the left and right sides is obtained as follows [26, 51, 52]:

$$\rho_{\mathrm{R}}(x_{\mathrm{DW}}) = 1 - \rho_{\mathrm{L}}(x_{\mathrm{DW}}), \tag{2.21}$$

where the x_{DW} denotes the position of the DW.

It is possible to determine the position of the DW in the steady state from (2.18), (2.19), and (2.21). If $\Delta = \rho_{\mathrm{R}}(x_{\mathrm{DW}}) - \rho_{\mathrm{L}}(x_{\mathrm{DW}}) > 0$ and $0 < x_{\mathrm{DW}} < 1$, we can find the DW.

2.3.3 Steady state

We show herein the phase diagram and the density profile for two examples in the original TASEP-LK.

The phase diagram is shown from the mean-field theory. In addition, we verify the accuracy of the density profile calculated from a mean-field theory by using Monte Carlo simulations.

2.3.3.1 $\Omega_{\mathrm{A}} = \Omega_{\mathrm{D}} = 0.3$

We examine the phase diagram and the density profile in the case that the attachment and detachment rates are equal.

Firstly, we reconsider a solution satisfied by the density profile in this especial case. When the attachment and detachment rates are equivalent, (2.16) is rewritten as follow:

$$\frac{\partial \rho}{\partial \bar{t}} = (1-2\rho)(\Omega - \frac{\partial \rho}{\partial x}), \tag{2.22}$$

where $\Omega := \Omega_{\mathrm{A}} = \Omega_{\mathrm{D}}$. In the steady state, we replace the $\partial\rho/\partial\bar{t}$ with 0. The equation has a trivial solution $\rho(x) = 1/2$. Another solution is obtained by

solving the following differential equation:

$$\frac{\mathrm{d}\rho}{\mathrm{d}x} = \Omega. \tag{2.23}$$

Since (2.23) can be easily integrated for the boundary conditions $\rho(0) = \alpha$ and $\rho(1) = 1 - \beta$, respectively, the left and right density profiles are the following equations:

$$\rho_{\mathrm{L}}(x) = \Omega x + \alpha, \tag{2.24}$$
$$\rho_{\mathrm{R}}(x) = \Omega(x-1) + 1 - \beta. \tag{2.25}$$

Therefore, we can represent explicitly the density profile by using the mean-field approximation in this special case.

Moreover, by using (2.21), (2.24), and (2.25), the position of the DW is given follows:

$$x_{\mathrm{DW}} = \frac{1}{2} + \frac{\beta - \alpha}{2\Omega}. \tag{2.26}$$

From (2.26), when the inflow rate α and outflow rate β are equivalent, the position of the DW is $x_{\mathrm{DW}} = 1/2$.

From the above, it is possible to make a prediction for the density profile. When the DW is observed, the profile is given by

$$\rho(x) = \begin{cases} \rho_{\mathrm{L}}(x) & (0 < x < x_{\mathrm{DW}}) \\ \rho_{\mathrm{R}}(x) & (x_{\mathrm{DW}} < x < 1) \end{cases} . \tag{2.27}$$

And the other density profile takes

$$\rho(x) = \begin{cases} \rho_{\mathrm{L}}(x) & (0 < x < x_1) \\ 1/2 & (x_1 < x < x_2) \\ \rho_{\mathrm{R}}(x) & (x_2 < x < 1) \end{cases} , \tag{2.28}$$

where the x_1 and x_2 are determined by $\rho_{\mathrm{L}}(x_1) = 1/2$ and $\rho_{\mathrm{R}}(x_2) = 1/2$, respectively. In this regard, if $x_1 < 0$ ($x_2 > 1$), $\rho_{\mathrm{L}}(x)$ ($\rho_{\mathrm{R}}(x)$) does not appear. In addition, the both boundaries are $\rho(0) = \alpha$ and $\rho(1) = 1 - \beta$, respectively.

Next, we show the phase diagram in Fig. 2.3. We can distinguish seven phases in the steady state. Firstly, as the three basic phases, the low-density phase (L), the high-density phase (H), and the maximum current phase (M)

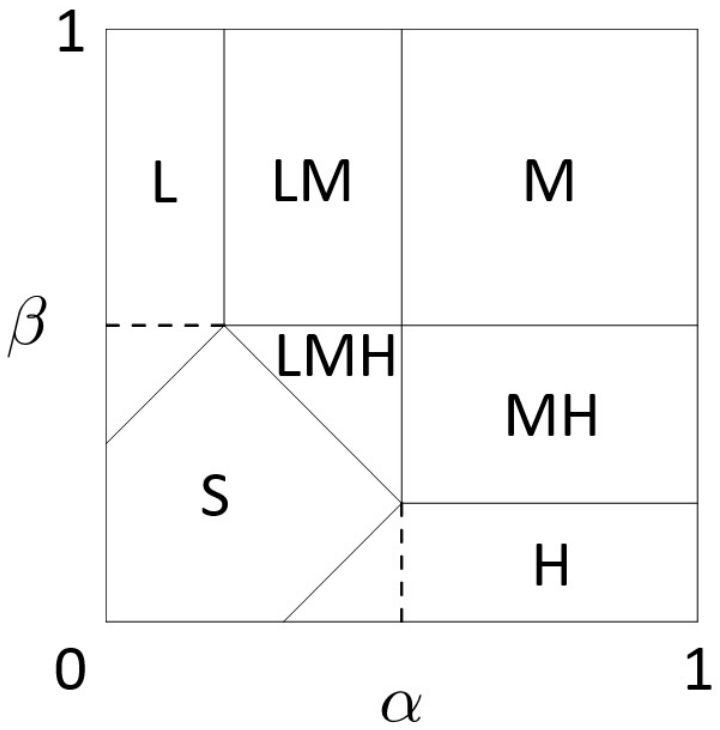

Figure 2.3: Phase diagram for $\Omega_A = \Omega_D = 0.3$. The low-density phase (L), the high-density phase (H), the shockwave phase (S), the maximum current phase (M), the coexistence of the low-density and maximum current phase (LM), the maximum current and high-density phase (MH), and the low-density, maximum current, and high-density phase (LMH) are indicated.

are observed. In the L (H), the density is lower (higher) than 1/2, and the density profile is expressed by $\rho_{\rm L}$ ($\rho_{\rm R}$). Then, in the M, the density is 1/2. This phase is called the maximum current phase because the flow is maximized at $\rho = 1/2$. In addition, as the coexistence phases, the shockwave phase (S), the low-density and maximum current phase (LM), the maximum current and high-density phase (MH), and the low-density, maximum current, and high-density phase (LMH) are observed. S is the phase where there exists a DW. In LH (MH), the density profile consists of $\rho_{\rm L}$ and 1/2 (1/2 and $\rho_{\rm R}$). In the LMH, the density profile consists of $\rho_{\rm L}$, 1/2, and $\rho_{\rm R}$.

Finally, we show the density profiles observed in each phase in Fig. 2.3. Figure 2.4 show the density profiles obtained by use of a mean-field approximation and performing Monte Carlo simulations. We performed Monte Carlo simulations with $L = 1000$ to obtain the density profile in the steady state. We find that the mean-field approximation and Monte Carlo simulation results are generally consistent.

2.3.3.2 $\Omega_{\rm A} = 0.2$ and $\Omega_{\rm D} = 0.1$

We examine the phase diagram and the density profile in the case that the attachment and detachment rates are unequal. The attachment rate and detachment rate are $\Omega_{\rm A} = 0.2$ and $\Omega_{\rm D} = 0.1$, respectively.

We show firstly the phase diagram in Fig. 2.5. We can distinguish three phases of the steady state. The low-density phase (L), the high-density phase (H), and the shockwave phase (S) are observed in Fig. 2.5. The solid lines and the chain lines show the shockwave phase boundaries.

Next, we explain the derivation method of the shockwave phase boundaries which separates the domain. The shockwave phase boundaries show the relation between α and β when DW is located at left and right ends.

When the DW is located at left end, the relational expression of left and right density satisfies $\rho_{\rm R}(0) = 1 - \rho_{\rm L}(0) = 1 - \alpha$ from (2.21). In other words, the relational expression of α and β for the shockwave phase boundary at this point (the position of the DW is the leftmost: $x_{\rm DW} = 0$) from (2.19) is as follows:

$$1 = \frac{2[1-\beta-(1-\alpha)]}{\Omega_{\rm A}+\Omega_{\rm D}} + \frac{\Omega_{\rm A}-\Omega_{\rm D}}{(\Omega_{\rm A}+\Omega_{\rm D})^2}\log\left|\frac{\Omega_{\rm A}-(\Omega_{\rm A}+\Omega_{\rm D})(1-\beta)}{\Omega_{\rm A}-(\Omega_{\rm A}+\Omega_{\rm D})(1-\alpha)}\right|. \tag{2.29}$$

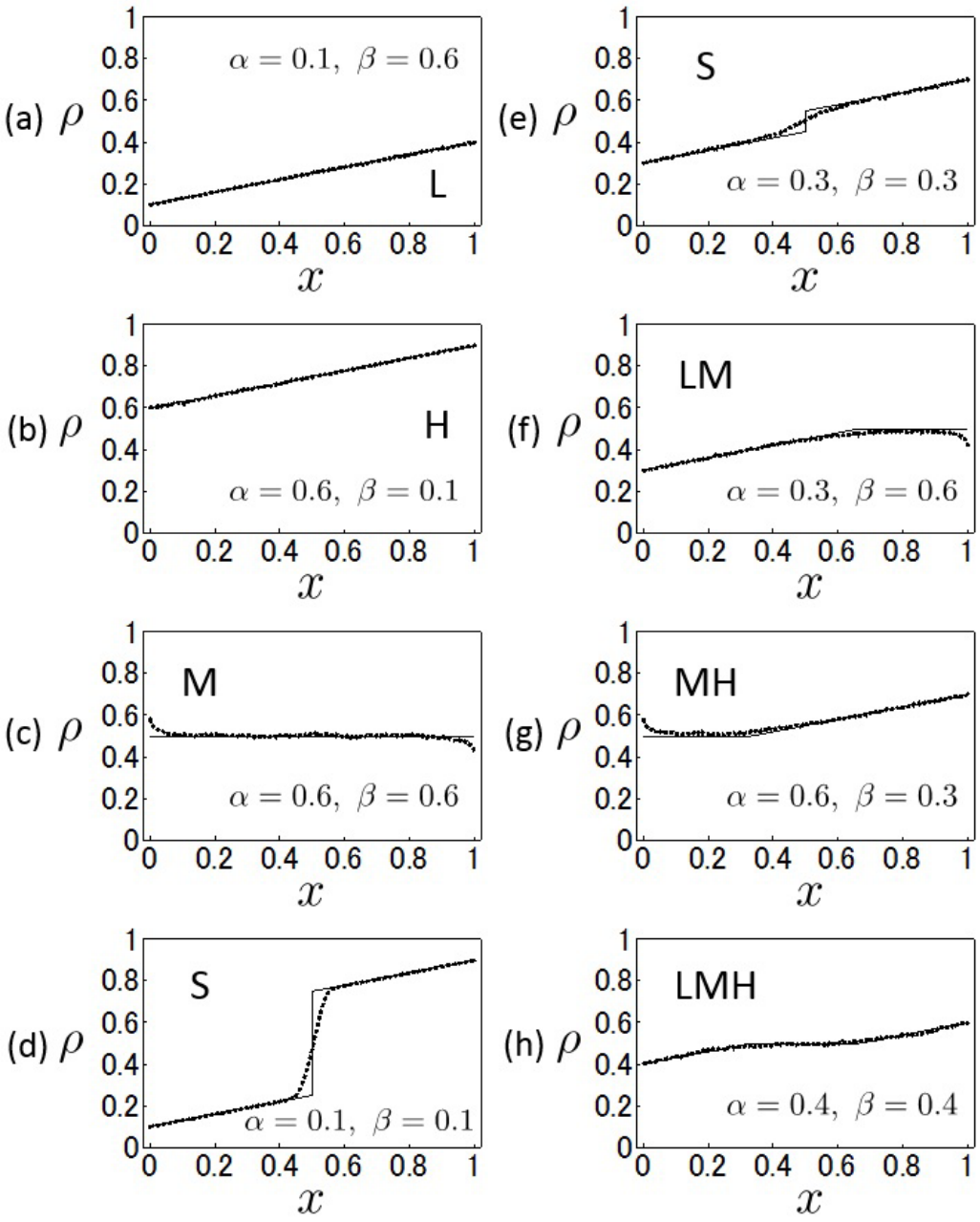

Figure 2.4: Density profile $\rho(x)$ for $\Omega_{\rm A} = \Omega_{\rm D} = 0.3$. Solid lines are the results using a mean-field approximation. Dotted lines are average density profiles computed by Monte Carlo simulations.

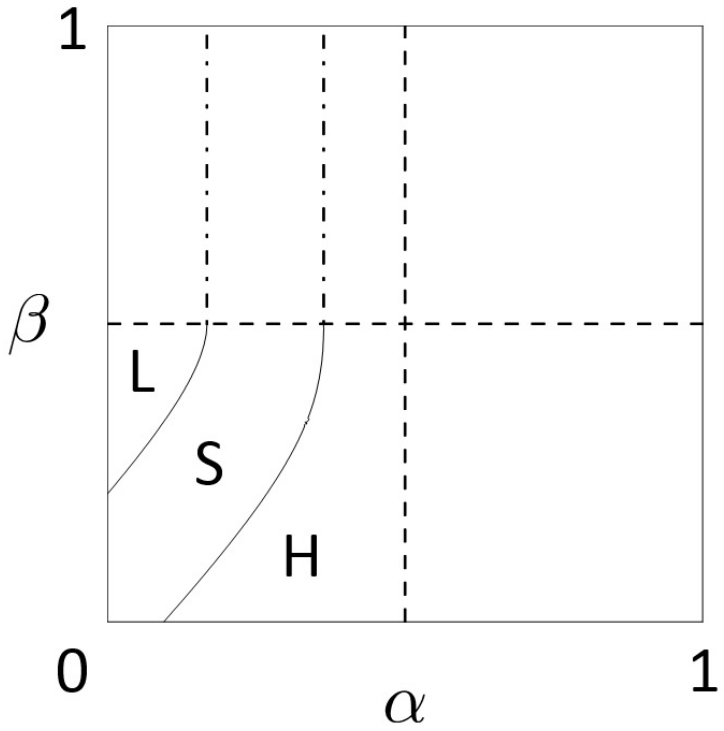

Figure 2.5: Phase diagram for $\Omega_A = 0.2$ and $\Omega_D = 0.1$. The low-density phase (L), the high-density phase (H), and the shockwave phase (S) are indicated.

Moreover, when the DW is located at right end, the relational expression of left and right density satisfies $1-\rho_{\mathrm{L}}(1) = \rho_{\mathrm{R}}(1) = 1-\beta$ from (2.21). Thus, the relational expression of α and β for the shockwave phase boundary at this point (the position of the DW is the rightmost: $x_{\mathrm{DW}} = 1$) from (2.18) is as follows:

$$1 = \frac{2(\beta-\alpha)}{\Omega_{\mathrm{A}}+\Omega_{\mathrm{D}}} + \frac{\Omega_{\mathrm{A}}-\Omega_{\mathrm{D}}}{(\Omega_{\mathrm{A}}+\Omega_{\mathrm{D}})^2}\log\Big|\frac{\Omega_{\mathrm{A}}-(\Omega_{\mathrm{A}}+\Omega_{\mathrm{D}})\beta}{\Omega_{\mathrm{A}}-(\Omega_{\mathrm{A}}+\Omega_{\mathrm{D}})\alpha}\Big|. \tag{2.30}$$

On the other hand, the chain lines cannot be drawn by calculating the equations in (2.29) and (2.30) as in the case of the solid lines. Those are the shockwave phase boundaries expected from the previous studies [12, 13] and the results of the simulations.

Finally, we show the density profiles in Fig. 2.6. Figure 2.6 show the density profiles obtained by use of a mean-field approximation and performing Monte Carlo simulations. The solid lines are the results using a mean-field approximation. The lines are obtained from numerical calculating (2.18), (2.19), and (2.21). In addition, the dotted lines show the density profile in the steady state obtained by performing Monte Carlo simulations with $L = 1000$. As is the case with 2.3.3.1, we can see that the mean-field approximation and Monte Carlo simulation results are generally consistent.

2.4 Summary

In this chapter, we reviewed the previous studies regarding the mathematical models we propose in this thesis. In particular, we introduced the results and the analytic methods for that in steady-state on the original TASEP-LK which is basis of our mathematical models.

Based on the analysis by Ezaki and Nishinari [32], we showed the exact stationary distribution on the original TASEP-LK with a periodic boundary. In addition, for the original TASEP-LK with an open boundaries, we explained that the density profile in the steady state was obtained analytically in high accuracy by using a mean-field approximation according to the results of Parmeggiani *et al.* [12] and Evans *et al* [13].

It is significant to analyze the steady state of the system mathematically in a rigorous manner. However, strict dealing with such a model is so challenging that it is impossible to find the solution easily. On the other hand, in the analysis with a mean-field approximation, while the correlations between

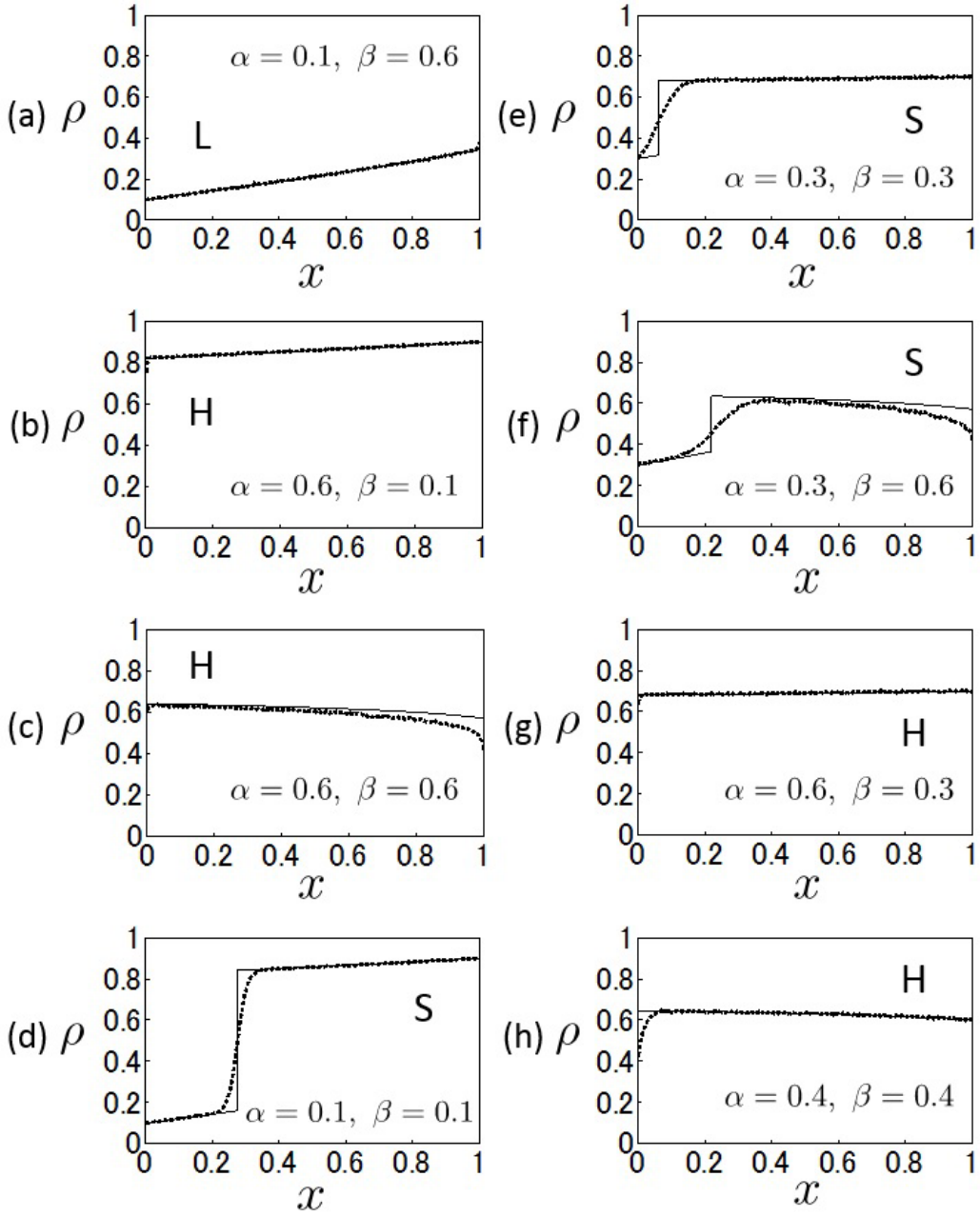

Figure 2.6: Density profile $\rho(x)$ for $\Omega_{\rm A} = 0.2$ and $\Omega_{\rm D} = 0.1$. Solid lines are the results using a mean-field approximation. Dotted lines are average density profiles computed by Monte Carlo simulations.

the states of the sites are ignored, we can treat the model analytically. Although attention to the accuracy of the approximation should be paid, the analytical method using a mean-field approximation is quite valuable for examination on the general structure of the system.

Chapter 3

Totally asymmetric simple exclusion process on a periodic lattice with Langmuir kinetics depending on the occupancy of the forward neighboring site

3.1 Preface

In this chapter*, we propose the mathematical model featuring the mechanism of attachment and detachment depending on the states of the forward neighboring space [33]. This model is devised against a background of the traffic flow with the lane changing shown as Fig. 1.2 in Sec. 1.2.

Generally speaking, when one changes the traffic lane, the wider the intruding spot and its forward space is, the more easily he changes. In addition, when the forward space becomes clogged for crowding on the driving road, consciousness for changing to the other lane is increasing. From this example, it is considered that analyzing mathematical model with the mechanism of attachment and detachment depending on the states of the forward neighboring space is valuable for capturing basic general structure of phenomena seen in actual.

*This chapter is composed of the contents partially modified based on [33]. The final publication of [33] is available at Springer via http://dx.doi.org/10.1140/epjb/e2016-70192-5.

We generalize the original TASEP-LK on a periodic lattice. Then, we analytically examine a density profile in the steady state and the relaxation dynamics by using a mean-field approximation in our model. Furthermore, we analyze some numerical examples, for example the case which is applicable to the feature of the traffic flow. For the original TASEP-LK with a periodic boundary, the exact stationary state [32] and the relaxation dynamics [53] have been presented.

3.2 Model

Let us consider a one-dimensional periodic lattice consisting of L sites ($L \geq 2$). Each site can either be empty ($\tau_i = 0$) or occupied by a single particle ($\tau_i = 1$). We assume that a particle can move to the site in front at rate 1 if it is vacant.

We describe the mechanism of attachment and detachment. In the original TASEP-LK, a simple mechanism of particle attachment and detachment is used. In contrast, in our model, the rates of attachment and detachment are classified into four cases according to the states of the forward neighboring site, as shown in Fig. 3.1. When the forward neighboring site is empty, the particle attachment and detachment rates are ω_{A_1} and ω_{D_1}, respectively. On the other hand, when the forward neighboring site is occupied, the attachment and detachment rates are ω_{A_2} and ω_{D_2}, respectively. We call this model "TASEP-LKF" in this thesis. We note that the TASEP-LK similar to our model with an open boundaries was proposed in [34, 43].

3.3 Analysis on model

We derive a density profile in the steady state and the relaxation time by using a mean-field approximation for the TASEP-LKF with a periodic boundary.

We firstly derive a differential equation satisfied by the density of the model. The time evolution of the probability distribution $P(\tau_1 \cdots \tau_L)$ of our

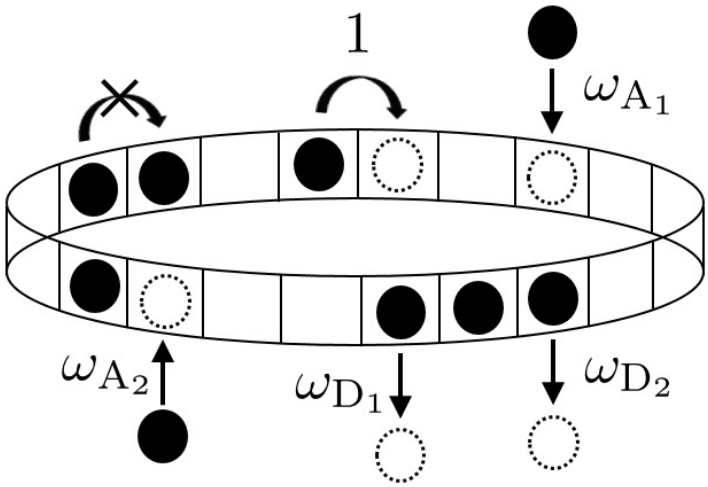

Figure 3.1: Schematic diagram of the TASEP-LKF with a periodic boundary.

model is described the following master equation

$$\begin{aligned}\frac{\mathrm{d}}{\mathrm{d}t}P(\tau_1\cdots\tau_L) = \sum_{i=1}^{L}\big[&(\tau_{i+1}-\tau_i)P(\tau_1\cdots\tau_{i-1}10\tau_{i+2}\cdots\tau_L)\\ &+\omega_{\mathrm{A}_1}(1-\tau_{i+1})(2\tau_i-1)P(\tau_1\cdots\tau_{i-1}00\tau_{i+2}\cdots\tau_L)\\ &+\omega_{\mathrm{A}_2}\tau_{i+1}(2\tau_i-1)P(\tau_1\cdots\tau_{i-1}10\tau_{i+2}\cdots\tau_L)\\ &-\omega_{\mathrm{D}_1}(1-\tau_{i+1})(2\tau_i-1)\tau_{i+1}P(\tau_1\cdots\tau_{i-1}01\tau_{i+2}\cdots\tau_L)\\ &-\omega_{\mathrm{D}_2}\tau_{i+1}(2\tau_i-1)P(\tau_1\cdots\tau_{i-1}11\tau_{i+2}\cdots\tau_L)\big].\end{aligned} \tag{3.1}$$

In a vector form this is simplified into

$$\frac{\mathrm{d}}{\mathrm{d}t}|P(t)\rangle = \mathcal{M}|P(t)\rangle, \tag{3.2}$$

where the Markov matrix $\mathcal{M}$ is given by

$$\mathcal{M} = \sum_{i=1}^{L}\mathcal{M}_{i,i+1}, \tag{3.3}$$

$$\mathcal{M}_{i,i+1} = \begin{pmatrix} -\omega_{\mathrm{A}_1} & 0 & \omega_{\mathrm{D}_1} & 0 \\ 0 & -\omega_{\mathrm{A}_2} & 1 & \omega_{\mathrm{D}_2} \\ \omega_{\mathrm{A}_1} & 0 & -\omega_{\mathrm{D}_1}-1 & 0 \\ 0 & \omega_{\mathrm{A}_2} & 0 & -\omega_{\mathrm{D}_2} \end{pmatrix}_{i,i+1}.$$

From the master equation, we can derive the evolution of the density at site i:

$$\begin{aligned}\frac{\mathrm{d}\langle\tau_i\rangle}{\mathrm{d}t} &= \langle\tau_{i-1}(1-\tau_i)\rangle - \langle\tau_i(1-\tau_{i+1})\rangle \\ &\quad + \omega_{\mathrm{A}_1}\langle(1-\tau_i)(1-\tau_{i+1})\rangle + \omega_{\mathrm{A}_2}\langle(1-\tau_i)\tau_{i+1}\rangle \\ &\quad - \omega_{\mathrm{D}_1}\langle\tau_i(1-\tau_{i+1})\rangle - \omega_{\mathrm{D}_2}\langle\tau_i\tau_{i+1}\rangle, \end{aligned} \tag{3.4}$$

where $\langle\cdot\rangle$ denotes the expected value of the quantity with respect to the probability distribution $P(\tau_1 \cdots \tau_L)$. By performing a mean-field approximation and ignoring the higher correlations in (3.4) [50], we obtain

$$\begin{aligned}\frac{\mathrm{d}\rho_i}{\mathrm{d}t} &= \rho_{i-1}(1-\rho_i) - \rho_i(1-\rho_{i+1}) \\ &\quad + \omega_{\mathrm{A}_1}(1-\rho_i)(1-\rho_{i+1}) + \omega_{\mathrm{A}_2}(1-\rho_i)\rho_{i+1} \\ &\quad - \omega_{\mathrm{D}_1}\rho_i(1-\rho_{i+1}) - \omega_{\mathrm{D}_2}\rho_i\rho_{i+1}, \end{aligned} \tag{3.5}$$

where ρ_i denotes the expected value $\langle\tau_i\rangle$. Since the density profile is spacially homogeneous in the steady state due to the translational invariance, we can replace ρ_{i-1}, ρ_i, and ρ_{i+1} in (3.5) with ρ after a sufficiently long time and obtain the following:

$$\frac{\mathrm{d}\rho}{\mathrm{d}t} = a\rho^2 + b\rho + c, \tag{3.6}$$

where $a := \omega_{\mathrm{A}_1} - \omega_{\mathrm{A}_2} + \omega_{\mathrm{D}_1} - \omega_{\mathrm{D}_2}$, $b := -2\omega_{\mathrm{A}_1} + \omega_{\mathrm{A}_2} - \omega_{\mathrm{D}_1}$, and $c := \omega_{\mathrm{A}_1}$.

Next, we classify this into the two cases and solve the differential equation (3.6) for the density profile.

In the one case, we consider the case of $a \neq 0$. Here we note that the discriminant

$$\begin{aligned} D :&= b^2 - 4ac \\ &= (\omega_{\mathrm{A}_2} - \omega_{\mathrm{D}_1})^2 + 4\omega_{\mathrm{A}_1}\omega_{\mathrm{D}_2} \end{aligned} \tag{3.7}$$

is always positive. It is possible to obtain a general solution by finding a particular solution. If ρ is in a steady state, we obtain $\mathrm{d}\rho/\mathrm{d}t = 0$. Thus, we find a particular solution when the left-hand side of (3.6) is replaced with 0

$$\rho_\pm := \frac{-b \pm \sqrt{D}}{2a}. \tag{3.8}$$

The general solution $\rho(t)$ can be obtained by using the particular solution $\rho_{\pm}$:

$$\rho(t) = \frac{\rho_- - \rho_+ C_1 e^{-\sqrt{D}t}}{1 - C_1 e^{-\sqrt{D}t}} \tag{3.9}$$

where C_1 denotes an integration constant. Since $\sqrt{D}$ is positive, we can obtain the following density profile in the steady state by setting $t \to \infty$:

$$\rho_\infty = \rho_-. \tag{3.10}$$

The values of ρ_- are always $0 \leq \rho_- \leq 1$ because $f(0) > 0$ and $f(1) < 0$, where $f(\rho) := a\rho^2 + b\rho + c$, and

$$\begin{cases} \rho_- < \rho_+ & \text{if} \quad a > 0 \\ \rho_- > \rho_+ & \text{if} \quad a < 0 \end{cases}. \tag{3.11}$$

Moreover, from (3.9), the relaxation time T is the following:

$$T^{-1} = \sqrt{D}. \tag{3.12}$$

In the other case, we consider the case of $a = 0$. In this case we have $b = -(\omega_{\mathrm{A}_1} + \omega_{\mathrm{D}_2}) < 0$. The differential equation (3.6) is rewritten in the form

$$\frac{\mathrm{d}\rho}{\mathrm{d}t} = -(\omega_{\mathrm{A}_1} + \omega_{\mathrm{D}_2})\rho + \omega_{\mathrm{A}_1}, \tag{3.13}$$

which yields the solution

$$\rho(t) = \frac{1}{1 + \omega_{\mathrm{D}_2}/\omega_{\mathrm{A}_1}} + C_2 e^{-(\omega_{\mathrm{A}_1} + \omega_{\mathrm{D}_2})t}, \tag{3.14}$$

where C_2 denotes an integration constant. In consequence, the density profile in the steady state and relaxation time are as follows:

$$\rho_\infty = \frac{1}{1 + \omega_{\mathrm{D}_2}/\omega_{\mathrm{A}_1}}, \quad T^{-1} = \omega_{\mathrm{A}_1} + \omega_{\mathrm{D}_2}. \tag{3.15}$$

3.4 Steady state

We examine a density profile of the TASEP-LKF with a periodic boundary in the steady state.

Firstly, we discuss an exact stationary probability distribution for the configurations of particles in a special case. The special case is that the attachment and detachment rates are set to be equal, i.e., $\omega_{\mathrm{A}_1} = \omega_{\mathrm{D}_1}$ and $\omega_{\mathrm{A}_2} = \omega_{\mathrm{D}_2}$. In this case, the master equation has the form

$$\begin{aligned}\frac{\mathrm{d}}{\mathrm{d}t}P(\tau_1\cdots\tau_L) = &\sum_{i=1}^{L}(\tau_{i+1}-\tau_i)P(\tau_1\cdots\tau_{i-1}10\tau_{i+2}\cdots\tau_L)\\ &+\sum_{i=1}^{L}\omega_1(2\tau_i-1)(1-\tau_{i+1})\big[P(\tau_1\cdots\tau_{i-1}00\tau_{i+2}\cdots\tau_L)\\ &\qquad -P(\tau_1\cdots\tau_{i-1}10\tau_{i+2}\cdots\tau_L)\big]\\ &+\sum_{i=1}^{L}\omega_2(2\tau_i-1)\tau_{i+1}\big[P(\tau_1\cdots\tau_{i-1}01\tau_{i+2}\cdots\tau_L)\\ &\qquad -P(\tau_1\cdots\tau_{i-1}11\tau_{i+2}\cdots\tau_L)\big],\end{aligned} \tag{3.16}$$

which has obviously the constant solution [26]

$$\bar{P}(\tau_1\cdots\tau_L) = \frac{1}{2^L}. \tag{3.17}$$

Each parameter in the master equation denotes $\omega_1 := \omega_{\mathrm{A}_1} = \omega_{\mathrm{D}_1}$, $\omega_2 := \omega_{\mathrm{A}_2} = \omega_{\mathrm{D}_2}$, and $\tau_{L+1} = \tau_1$. Therefore, the average density at site i is obtained as follows:

$$\langle\tau_i\rangle = \frac{\sum_{N=1}^{L}{}_{L-1}C_{N-1}\times 1/2^L}{\sum_{N=0}^{L}{}_{L}C_{N}\times 1/2^L} = \frac{1}{2}, \tag{3.18}$$

where N denotes the number of particles for given configuration. Thus, the density profile is $1/2$ in the steady state.

Next, we show the density profiles in the steady state by use of Monte Carlo simulations in the general cases. We perform Monte Carlo simulations with $L = 100$. Here, the following four cases are considered in Table 3.1. Both (A) and (C) show the case of $\omega_{\mathrm{A}_1} > \omega_{\mathrm{A}_2}$ and $\omega_{\mathrm{D}_2} > \omega_{\mathrm{D}_1}$, and both (B) and (D) show the case of $\omega_{\mathrm{A}_2} > \omega_{\mathrm{A}_1}$ and $\omega_{\mathrm{D}_1} > \omega_{\mathrm{D}_2}$. In the case of $\omega_{\mathrm{A}_1} > \omega_{\mathrm{A}_2}$ and $\omega_{\mathrm{D}_2} > \omega_{\mathrm{D}_1}$, they show that it is easy to attach when the forward site is vacant, on the other hand it is easy to detach when the forward site is

	ω_{A_1}	ω_{D_1}	ω_{A_2}	ω_{D_2}
(A)	0.008	0.001	0.002	0.004
(B)	0.002	0.004	0.008	0.001
(C)	0.004	0.002	0.001	0.008
(D)	0.001	0.008	0.004	0.002

Table 3.1: Attachment and detachment rates.

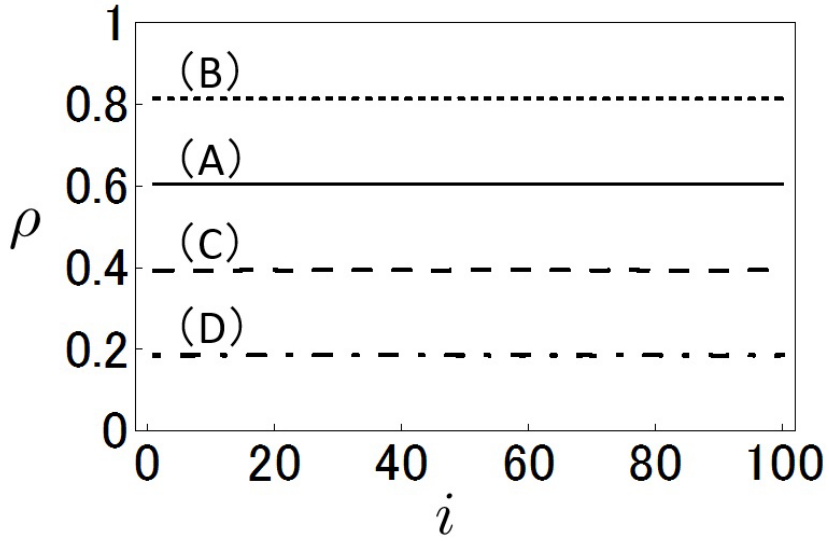

Figure 3.2: Density profile ρ computed by Monte Carlo simulations for (A), (B), (C), and (D).

occupied. Moreover, we define the attachment and detachment ratio as $r := (\omega_{A_1}+\omega_{A_2})/(\omega_{D_1}+\omega_{D_2})$, and we set $r(\mathrm{A}) = r(\mathrm{B}) = 2$ and $r(\mathrm{C}) = r(\mathrm{D}) = 1/2$. Namely, (A) and (B) show the case that the attachment effect is higher than the detachment effect ($r > 1$). On the other hand (C) and (D) show the contrary case ($r < 1$). Comparing the four cases (A), (B), (C), and (D), we can capture the characteristic which the mechanism of attachment and detachment give to the density profile.

In Fig. 3.2, we show the density profiles of (A), (B), (C), and (D) in the steady state computed from Monte Carlo simulations. The density tends to be high when the attachment effect is higher than the detachment effect ($r > 1$). In addition, when we compare the case (A) with (B), the density is

lower in (A). In the same way, in the comparison of (C) with (D), the density is higher in (C). Therefore, we find that the density gets closer to 1/2 in the case of $\omega_{\mathrm{A}_1} > \omega_{\mathrm{A}_2}$ and $\omega_{\mathrm{D}_2} > \omega_{\mathrm{D}_1}$ even if attachment and detachment ratio r is the same value. Since the flow $J = \rho(1-\rho)$ is maximized at $\rho = 1/2$, this means that particles flow more efficiently than in the case of $\omega_{\mathrm{A}_2} > \omega_{\mathrm{A}_1}$ and $\omega_{\mathrm{D}_1} > \omega_{\mathrm{D}_2}$.

For example, in the case of the traffic flow, it is easy to change the lane when the forward is vacant as a space for cutting in for the driving direction. By contrast, when it becomes stuffed in the forward direction, this situation makes us change to another lane mentally. This example corresponds to the case of $\omega_{\mathrm{A}_1} > \omega_{\mathrm{A}_2}$ and $\omega_{\mathrm{D}_2} > \omega_{\mathrm{D}_1}$. Thus, we are able to interpret these observations as meaning that drivers move naturally so as to increase the flow. This discussion suits the physical intuition.

Finally, we compare between the results using a mean-field approximation and Monte Carlo simulations in the steady state. Table 3.2 shows the densities calculated from a mean-field theory (3.10) (MF) and Monte Carlo simulations (MC). The values of MC are the average densities and standard error for simulations of 100 times. We find that both of them are consistent to an accuracy of 2 digits. There are slight gaps between the numerical values of densities for MF and MC. We consider that is because Monte Carlo simulations are performed with finite size L.

	Density (MF)	Density (MC)
(A)	0.607031	0.605652 ± 0.000015
(B)	0.816497	0.813911 ± 0.000032
(C)	0.392969	0.394333 ± 0.000017
(D)	0.183503	0.185982 ± 0.000035

Table 3.2: Density in the steady state calculated from a mean-field theory (3.10) (MF) and Monte Carlo simulations (MC).

3.5 Relaxation dynamics

We examine the relaxation dynamics in the case of (A) and (B) in Table 3.1.

Firstly, we show the relaxation times obtained by using a mean-field approximation (MF) in Table 3.3.

	Relaxation time (A)	Relaxation time (B)
MF	88.0451	204.124

Table 3.3: Relaxation times calculated from a mean-field theory (MF).

Secondly, performing the Monte Carlo simulations with $L = 100$, we numerically estimate the relaxation time from the time evolution of the number of particles starting from some initial state. We consider the initial states as following: (a) no particle in all sites, (b) particles in all sites, (c) particles in the left half and no particle in the right half in the lattice sites, and (d) particles placed alternately ($\tau_{2n-1} = 0, \tau_{2n} = 1$).

Figures 3.3 and 3.4 show the relaxation dynamics of the density ρ in the case of (A) and (B), respectively. The dotted curves are obtained from (3.9). Then, the solid gray curves represent the time evolution of the average density from Monte Carlo simulation 1000 times.

Moreover, we numerically estimate the relaxation time T by the fitting function

$$\rho(t) = \rho_\infty - (\rho_\infty - \rho_0)e^{-\frac{t}{T}} \tag{3.19}$$

with the fitting parameters ρ_∞ and T. As for the density in the steady state ρ_∞, we use the average value of MC in Table 3.2. In addition, ρ_0 denotes the spacial average of density in the initial state. In consequence, we numerically obtain the relaxation times of (A) and (B) as shown Fig. 3.4.

	Relaxation time (A)	Relaxation time (B)
(a)	80.7998	293.653
(b)	93.2934	194.991
(c)	71.4181	249.510
(d)	88.6798	225.987

Table 3.4: Relaxation times calculated from Monte Carlo simulations.

Finally, in the case of small systems up to $L = 14$, we calculate the second largest eigenvalue of the Markov matrices (3.3) by the exact diagonalization, which is equal to the inverse of the relaxation time. We have extrapolated the data by $c_0 + c_1/L$ and estimated the values in $L \to \infty$ by c_0. In Fig. 3.5, the solid lines are fitting lines $c_0 + c_1/L$. Therefore, the intercepts of linear approximation lines are the relaxation times in $L \to \infty$. In Table 3.5, we

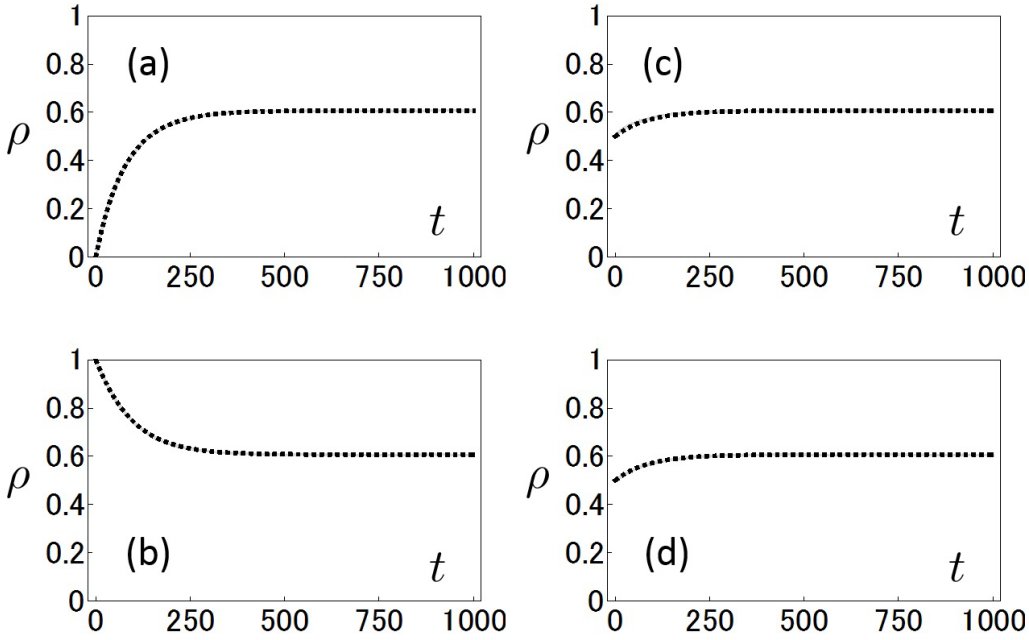

Figure 3.3: The relationship between the time t and the density ρ for (A). The solid gray curves (MC) are the average of density data obtained by performing Monte Carlo simulation 1000 times. The dotted curves (MF) are the density change obtained from a mean-field approximation.

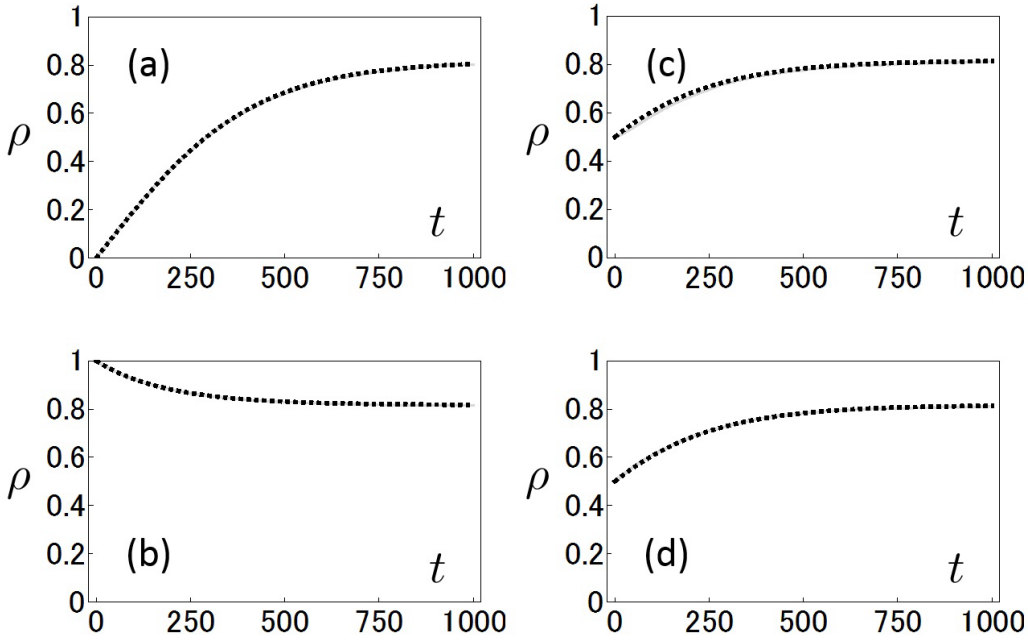

Figure 3.4: The relationship between the time t and the density ρ for (B). The solid gray curves (MC) are the average of density data obtained by performing Monte Carlo simulation 1000 times. The dotted curves (MF) are the density change obtained from a mean-field approximation.

show the relaxation times of (A) and (B) obtained from the extrapolations.

	Relaxation time (A)	Relaxation time (B)
ED	88.0219	200.907

Table 3.5: Relaxation times calculated from the exact diagonalization (ED).

From the above results, we verify the accuracy of the relaxation time calculated from a mean-field theory. From Figs. 3.3, 3.4, and 3.5, one can see that the mean-field approximation well describe the relaxation dynamics. However, there are slight gaps between the numerical values of relaxation times for MF and MC. We can think following two reasons.

Firstly, we assume the spatial homogeneity of the density profile in obtaining the analytical expression of the relaxation time by using the mean field approximation. On the other hand, the attachment and detachment rate that gives a strong effect on the dynamics varies depending on the configuration of particles in the system. We consider that this spatial dependence induces the slight difference in the relaxation dynamics for MF and MC.

Secondly, the value of MC is derived from the fitting using the function of the standard exponential relaxation. We neglect the higher order correction terms in the relaxation process, which induces the variability in the fitting value of relaxation time for MC.

3.6 Summary

In this chapter, we studied the TASEP-LK model on a periodic lattice with a distinction that the rates of attachment and detachment depend on the states of the forward neighboring site. Then, the density profile in the steady state and the relaxation dynamics were analyzed by using a mean-field approximation, Monte Carlo simulations and the exact diagonalization.

In consequence, we could obtain the analytical expression of the density profile in the steady state and the relaxation time by using a mean-field approximation. Therefore, we succeeded in obtaining analytically the expression of the dynamics in our model.

We claim that our model has a potential for applying to actual phenomena. Actually it describes, despite its simplicity, the basic characteristics of

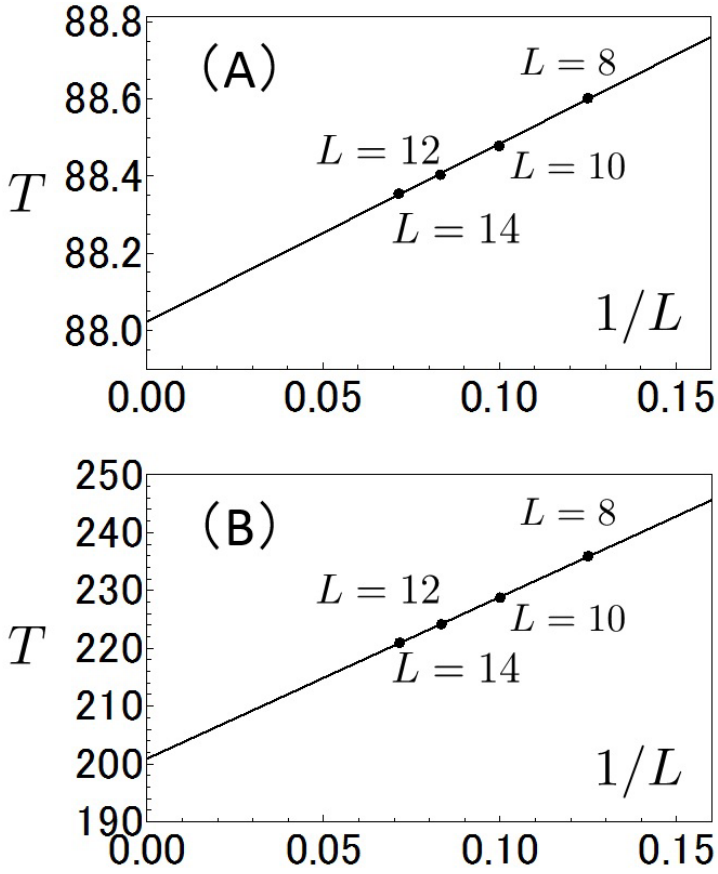

Figure 3.5: Relaxation time T for (A) and (B) obtained from the exact diagonalization is plotted against the inverse of the system size $1/L$. The solid line is linear approximation for the relaxation times in the cases of $L = 8$, 10, 12, and 14. The extrapolated values for (A) and (B) are 88.0219 and 200.907, respectively.

lane-changing in the multi-lane traffic flow in accordance with the physical intuition.

Since there have been many previous studies in this field [14], it will be expected to reveal in more detail the structure of the dynamics of traffic jam by incorporating their results in our model.

Chapter 4

Totally asymmetric simple exclusion process on an open lattice with Langmuir kinetics depending on the occupancy of the forward and backward neighboring sites

4.1 Preface

In this chapter[†], we study the TASEP-LK with rates of attachment and detachment depending on the states of the neighboring sites [34]. We think LK which has more complex interaction than the model that we have studied in Chap. 3 by considering additionally the state of each backward site as well. Additionally, in contrast to the case in Chap. 3, we think the model with an open boundaries. As it is known in the original TASEP-LK, we can observe more rich phenomena in the model with an open boundaries than the case of a periodic boundary. On the other hand, through considering the open boundaries, it becomes difficult to analyze the model mathematically. Thus, we here analyze the model about the case where the attachment rate

[†]This chapter is composed of the contents partially modified based on [34]. The final publication of [34] is available at the Physical Society of Japan via http://doi.org/10.7566/JPSJ.85.044001.

and the detachment rate are equal. Then, we explicitly capture the density profiles in the steady state by using a mean-field approximation. In addition, we analyze how the extended LK influences the system. If the general structure in the system with more complex LK is mathematically revealed, it is considered to be useful for understanding the various complex systems that we have given as the examples in 1.2.

Vuijk *et al.* has recently studied a closely related model [43]. We explain with comparison on the difference between our model and their model.

4.2 Model

Let us consider a one-dimensional open lattice consisting of L sites ($L \geq 3$). We assume that a particle can move to the site in front at rate 1 if it is vacant.

We describe the mechanism of attachment and detachment. In the original TASEP-LK, a simple mechanism of particle attachment and detachment is used, i.e., a particle attaches to a site with a certain rate if the site is vacant, whereas a particle is detached from a site with a certain rate if the site is occupied. In contrast, in our model, the rates of attachment and detachment are classified into four cases according to the states of two neighboring sites, as shown in Fig. 4.1. In the first case, where both neighboring sites are empty, particles attach and detach at rate ω_1, as shown in Fig. 4.1 (a). Next, we consider the case where one of neighboring sites is occupied by a single particle. In the one case, where the forward neighboring site is occupied, the attachment and detachment rates are ω_{21}, as shown in Fig. 4.1 (b). In the other case, where the backward neighboring site is occupied, the attachment and detachment rates are ω_{22}, as shown in Fig. 4.1 (c). Finally, when both neighboring sites are occupied, the attachment and detachment rates are ω_3, as shown in Fig. 4.1 (d). We call the model with the foregoing LK "TASEP-LKFB" in this thesis.

Similarly, the boundary conditions are affected by this generalization, as shown in Fig. 4.2. A particle flows into the leftmost site at the rate α (inflow rate). In addition, we consider the detachment of the particle from the leftmost site depending on the occupancy of the second site from the left. When the second site from the left does not contain a particle, a particle detaches at the rate ω_1, whereas a particle detaches at the rate ω_{21} when there is a particle in the second site from the left. In the same manner, at the right boundary, a particle flows out from the rightmost site at the

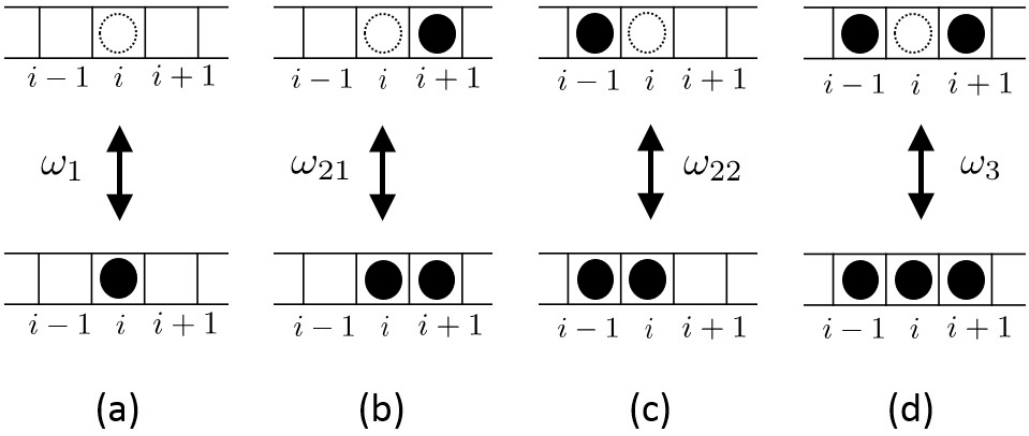

Figure 4.1: (a) No particle is on either neighboring site. (b) There is a particle on the right site. (c) There is a particle on the left site. (d) Both neighboring sites are occupied.

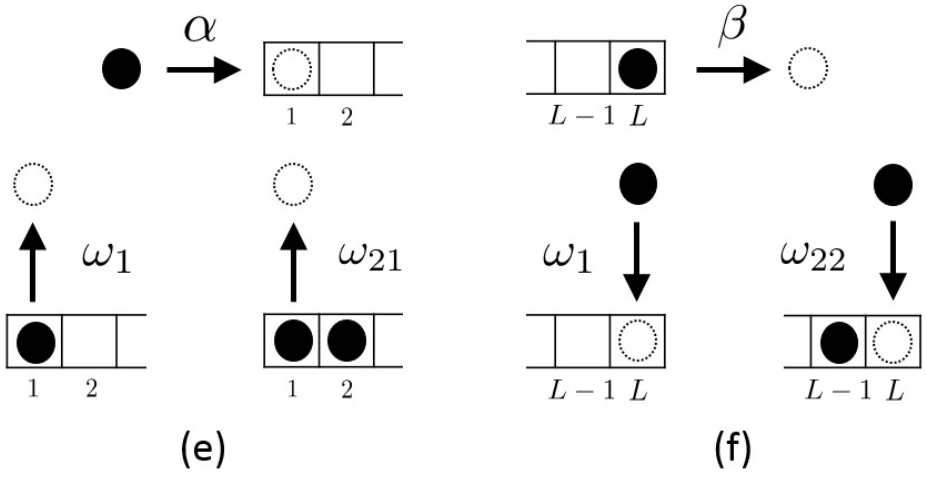

Figure 4.2: (e) Left boundary condition. (f) Right boundary condition.

rate β (outflow rate). In addition, we consider the attachment of particles in the rightmost site depending on the occupancy of the second site from the right. When the second site from the right does not have a particle, a particle attaches at the rate ω_1, whereas a particle attaches at the rate ω_{22} when there is a particle in the second site from the right.

Recently, a closely related model has been studied by Vuijk *et al.* [43] The difference from their model is that we more finely classify the states of the neighboring sites, and each rate in which the attachment rate and detachment rate are equal can take arbitrary values independently in our model.

4.3 Analysis on model

We obtain explicitly the solutions satisfied the density profile by using a mean-field approximation in this section.

4.3.1 Mean-field approximation and hydrodynamic limit

We derive a partial differential equation satisfied by the density profile of this model. Each site can either be empty ($\tau_i = 0$) or occupied by a single particle ($\tau_i = 1$). At site i, the following equation can be expressed from the master equation:

$$\begin{aligned}\frac{\mathrm{d}\langle\tau_i\rangle}{\mathrm{d}t} &= \langle\tau_{i-1}(1-\tau_i)\rangle - \langle\tau_i(1-\tau_{i+1})\rangle \\ &\quad + \omega_1\langle(1-\tau_{i-1})(1-\tau_i)(1-\tau_{i+1})\rangle \\ &\quad + \omega_{21}\langle(1-\tau_{i-1})(1-\tau_i)\tau_{i+1}\rangle \\ &\quad + \omega_{22}\langle\tau_{i-1}(1-\tau_i)(1-\tau_{i+1})\rangle + \omega_3\langle\tau_{i-1}(1-\tau_i)\tau_{i+1}\rangle \\ &\quad - \omega_1\langle(1-\tau_{i-1})\tau_i(1-\tau_{i+1})\rangle - \omega_{21}\langle(1-\tau_{i-1})\tau_i\tau_{i+1}\rangle \\ &\quad - \omega_{22}\langle\tau_{i-1}\tau_i(1-\tau_{i+1})\rangle - \omega_3\langle\tau_{i-1}\tau_i\tau_{i+1}\rangle, \end{aligned} \tag{4.1}$$

where $\langle\cdot\rangle$ denotes the expectation value of the quantity. In addition, the equation for the boundary is as follows:

$$\begin{aligned}\frac{\mathrm{d}\langle\tau_1\rangle}{\mathrm{d}t} &= \alpha\langle 1-\tau_1\rangle - \langle\tau_1(1-\tau_2)\rangle \\ &\quad - \omega_1\langle\tau_1(1-\tau_2)\rangle - \omega_{21}\langle\tau_1\tau_2\rangle. \qquad (4.2)\\ \frac{\mathrm{d}\langle\tau_L\rangle}{\mathrm{d}t} &= \langle\tau_{L-1}(1-\tau_L)\rangle - \beta\langle\tau_L\rangle \\ &\quad + \omega_1\langle(1-\tau_{L-1})(1-\tau_L)\rangle + \omega_{22}\langle\tau_{L-1}(1-\tau_L)\rangle. \qquad (4.3)\end{aligned}$$

Then, we perform a mean-field approximation in (4.1). In other words, we factor the correlation functions by replacing $\langle\tau_i(1-\tau_{i+1})\rangle$ with $\langle\tau_i\rangle(1-\langle\tau_{i+1}\rangle)$ [50]. Moreover, we perform the hydrodynamic limit. The expectation value $\langle\tau_{i\pm1}\rangle$ is expanded as:

$$\langle\tau_{i\pm1}\rangle = \rho(x) \pm \frac{1}{L}\frac{\partial\rho}{\partial x} + \frac{1}{2}\frac{1}{L^2}\frac{\partial^2\rho}{\partial x^2} + \mathcal{O}\left(\frac{1}{L^3}\right). \qquad (4.4)$$

Substituting the first and second terms of this into (4.1), we obtain the following partial differential equation by setting $t = \bar{t}L$ and $L \to \infty$:

$$\begin{aligned}\frac{\partial\rho}{\partial\bar{t}} + (1-2\rho)\frac{\partial\rho}{\partial x} &= (1-2\rho) \\ &\quad \times \left[\Omega_1(1-\rho)^2 + (\Omega_{21}+\Omega_{22})\rho(1-\rho) + \Omega_3\rho^2\right], \qquad (4.5)\end{aligned}$$

where $\Omega_1 = \omega_1 L$, $\Omega_{21} = \omega_{21}L$, $\Omega_{22} = \omega_{22}L$, and $\Omega_3 = \omega_3 L$ are kept finite.

4.3.2 Steady-state solution

We find a solution for the density in the steady state from the partial differential equation (4.5). In the steady state, the density does not change with respect to time. Thus, we replace the $\partial\rho/\partial\bar{t}$ in (4.5) with 0 and solve this differential equation for the position and density. The equation has a trivial solution $\rho(x) = 1/2$. Another solution is obtained by solving the following differential equation:

$$\begin{aligned}\frac{\mathrm{d}\rho}{\mathrm{d}x} &= \Omega_1(1-\rho)^2 + (\Omega_{21}+\Omega_{22})\rho(1-\rho) + \Omega_3\rho^2 \\ &= [\Omega_1 - (\Omega_{21}+\Omega_{22}) + \Omega_3]\rho^2 \\ &\quad + [-2\Omega_1 + (\Omega_{21}+\Omega_{22})]\rho + \Omega_1. \qquad (4.6)\end{aligned}$$

Firstly, we consider the case of $\Omega_1 - (\Omega_{21} + \Omega_{22}) + \Omega_3 = 0$. The solution $\rho(x)$ can be obtained as follows:

$$\rho(x) = C_1 e^{bx} - \frac{c}{b}, \tag{4.7}$$

where $b := -2\Omega_1 + (\Omega_{21} + \Omega_{22})$, $c := \Omega_1$, and C_1 denotes an integration constant. Since the left and right boundary conditions are $\rho(0) = \alpha$ and $\rho(1) = 1 - \beta$, the left (right) neighborhood solution $\rho_{\mathrm{L}}(x)$ ($\rho_{\mathrm{R}}(x)$) are as follows:

$$\rho_{\mathrm{L}}(x) = \left(\alpha + \frac{c}{b}\right) e^{bx} - \frac{c}{b}. \tag{4.8}$$

$$\rho_{\mathrm{R}}(x) = \left[(1 - \beta) + \frac{c}{b}\right] e^{b(x-1)} - \frac{c}{b}. \tag{4.9}$$

Next, we consider below the case of $\Omega_1 - (\Omega_{21} + \Omega_{22}) + \Omega_3 \neq 0$. If $\rho(x)$ is constant, we obtain $\mathrm{d}\rho/\mathrm{d}x = 0$. Thus, we find a particular solution when the left-hand side of (4.6) is replaced with 0:

$$\xi_{\pm} = \frac{2\Omega_1 - (\Omega_{21} + \Omega_{22}) \pm \sqrt{(\Omega_{21} + \Omega_{22})^2 - 4\Omega_1\Omega_3}}{2[\Omega_1 - (\Omega_{21} + \Omega_{22}) + \Omega_3]}. \tag{4.10}$$

In the case of $(\Omega_{21} + \Omega_{22})^2 - 4\Omega_1\Omega_3 > 0$, the solution $\rho(x)$ can be obtained as follow:

$$\rho(x) = \frac{\xi_+ - \xi_- C_2 e^{a(\xi_+ - \xi_-)x}}{1 - C_2 e^{a(\xi_+ - \xi_-)x}}, \tag{4.11}$$

where $a = \Omega_1 - (\Omega_{21} + \Omega_{22}) + \Omega_3$. In addition, C_2 is an integration constant determined from each boundary condition. From the both boundary conditions, the left and right neighborhood solutions are as follows:

$$\rho_{\mathrm{L}}(x) = \frac{\xi_+(\xi_- - \alpha) - \xi_-(\xi_+ - \alpha)e^{a(\xi_+ - \xi_-)x}}{(\xi_- - \alpha) - (\xi_+ - \alpha)e^{a(\xi_+ - \xi_-)x}}, \tag{4.12}$$

$$\rho_{\mathrm{R}}(x) = \frac{\xi_+[\xi_- - (1 - \beta)] - \xi_-[\xi_+ - (1 - \beta)]e^{a(\xi_+ - \xi_-)(x-1)}}{[\xi_- - (1 - \beta)] - [\xi_+ - (1 - \beta)]e^{a(\xi_+ - \xi_-)(x-1)}}. \tag{4.13}$$

In the case of $(\Omega_{21} + \Omega_{22})^2 - 4\Omega_1\Omega_3 < 0$, the solution $\rho(x)$ can be written as:

$$\rho(x) = u + v \tan[avx - C_3], \tag{4.14}$$

where we put $\xi_\pm = u \pm \mathrm{i}v$ and C_3 denotes an integration constant. From the both boundary conditions, the left and right neighborhood solutions are as follows:

$$\rho_{\mathrm{L}}(x) = u + v\tan\Big[avx + \arctan\Big[\frac{\alpha - u}{v}\Big]\Big], \tag{4.15}$$

$$\rho_{\mathrm{R}}(x) = u + v\tan\Big[av(x-1) + \arctan\Big[\frac{(1-\beta) - u}{v}\Big]\Big]. \tag{4.16}$$

In the case of $(\Omega_{21}+\Omega_{22})^2 - 4\Omega_1\Omega_3 = 0$, the solution $\rho(x)$ can be expressed as follows:

$$\rho(x) = \frac{1 + \xi(C_4 - ax)}{C_4 - ax}, \tag{4.17}$$

where $\xi := \xi_+ = \xi_-$ and C_4 denotes an integration constant. From the both boundary conditions, the following are the left and right neighborhood solutions:

$$\rho_{\mathrm{L}}(x) = \frac{\alpha + \xi a(\xi - \alpha)x}{1 + a(\xi - \alpha)x}, \tag{4.18}$$

$$\rho_{\mathrm{R}}(x) = \frac{(1-\beta) + \xi a[\xi - (1-\beta)](x-1)}{1 + a[\xi - (1-\beta)](x-1)}. \tag{4.19}$$

One of the solutions shown by Vuijk *et al.* is included in this case [43].

Next, we consider the discontinuity (DW) in the density profile described by the original TASEP-LK [12,13]. As with the original TASEP-LK, we have the following relational expression at the position of DW [26, 51, 52].

$$\rho_{\mathrm{R}}(x_{\mathrm{DW}}) = 1 - \rho_{\mathrm{L}}(x_{\mathrm{DW}}). \tag{4.20}$$

Therefore, it is possible to determine the position of the DW in the steady state from ρ_{L}, ρ_{R}, and (4.20). If $\Delta = \rho_{\mathrm{R}}(x_{\mathrm{DW}}) - \rho_{\mathrm{L}}(x_{\mathrm{DW}}) > 0$ and $0 < x_{\mathrm{DW}} < 1$, we can find the DW.

Thus, when the DW is observed, the density profile is given by

$$\rho(x) = \begin{cases} \rho_{\mathrm{L}}(x) & (0 < x < x_{\mathrm{DW}}), \\ \rho_{\mathrm{R}}(x) & (x_{\mathrm{DW}} < x < 1). \end{cases} \tag{4.21}$$

And the other density profile takes

$$\rho(x) = \begin{cases} \rho_{\mathrm{L}}(x) & (0 < x < x_1), \\ 1/2 & (x_1 < x < x_2), \\ \rho_{\mathrm{R}}(x) & (x_2 < x < 1), \end{cases} \tag{4.22}$$

where the x_1 and x_2 are determined by $\rho_{\mathrm{L}}(x_1) = 1/2$ and $\rho_{\mathrm{R}}(x_2) = 1/2$, respectively. In this regard, if $x_1 < 0$ ($x_2 > 1$), $\rho_{\mathrm{L}}(x)$ ($\rho_{\mathrm{R}}(x)$) does not appear. In addition, the both boundaries are $\rho(0) = \alpha$ and $\rho(1) = 1 - \beta$, respectively.

4.4 Steady state

We analyze the behavior of the TASEP-LKFB in the steady state.

Hereafter we set $\Omega_2 := \Omega_{21} = \Omega_{22}$ ($2\Omega_2 = \Omega_{21} + \Omega_{22}$), because only the term $\Omega_{21} + \Omega_{22}$ appears in the density profile as is seen in the steady-state solutions. Moreover, if the value of the sum is the same, even each value of Ω_{21} and Ω_{22} is changing, it is confirmed by Monte Carlo simulations that the density profile does not change as long as the system size L is sufficiently large. Despite the asymmetricity of our model, it is a point of interest that the value of each Ω_{21} and Ω_{22} does not affect the density profile as long as the sum $\Omega_{21} + \Omega_{22}$ is kept constant.

4.4.1 Phase diagram

We show the phase diagram in Fig. 4.3 for $\Omega_1 = 0.3$, $\Omega_2 = 0.4$, and $\Omega_3 = 0.2$ as a representative of the attachment and detachment parameters. The phase diagram is shown from the mean-field theory.

We can distinguish seven phases of the steady state as with the case of 2.3.3.1 in the original TASEP-LK. Firstly, as the three basic phases, the low-density phase (L), the high-density phase (H), and the maximum current phase (M) are observed. In L (H), the density is lower (higher) than 1/2, and the density profile is expressed by ρ_{L} (ρ_{R}). Then, in M, the density is 1/2. This phase is called the maximum current phase because the flow is maximized at $\rho = 1/2$. In addition, as the coexistence phases, the shockwave phase (S), the low-density and maximum current phase (LM), the maximum current and high-density phase (MH), and the low-density, maximum current, and high-density phase (LMH) are observed. S is the phase where there exists a DW. In LM (MH), the density profile consists of ρ_{L} and 1/2 (1/2 and ρ_{R}). In LMH, the density profile consists of ρ_{L}, 1/2, and ρ_{R}.

In addition, we can see that the shape of the shockwave phase is distorted from Fig. 4.3. The lines l_0 and l_1 correspond to the phase boundaries for $x_{\mathrm{DW}} = 0$ and $x_{\mathrm{DW}} = 1$, respectively. The dotted lines indicate the phase

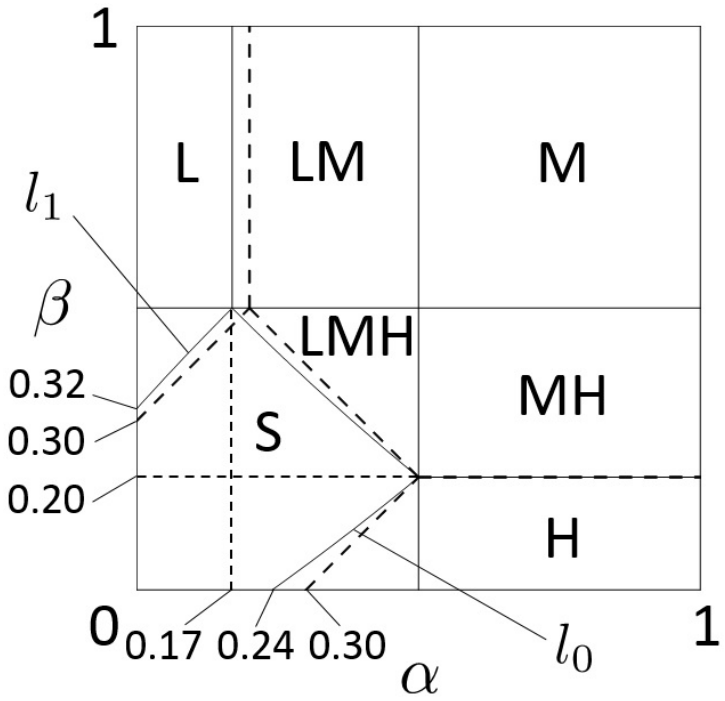

Figure 4.3: Phase diagram for $\Omega_1 = 0.3$, $\Omega_2 = 0.4$, and $\Omega_3 = 0.2$. The high-density phase (H), the low-density phase (L), the maximum current phase (M), the shockwave phase (S), the coexistence of the maximum current and high-density phase (MH), the low-density and maximum current phase (LM), and the low-density, maximum current, and high-density phase (LMH) are indicated. The line l_0 is the phase boundary for $x_{\mathrm{DW}} = 0$, and the line l_1 is the phase boundary for $x_{\mathrm{DW}} = 1$. In addition, the dotted lines indicate the phase boundaries for $\Omega_1 = \Omega_2 = \Omega_3 = 0.3$. The values are rounded off to the second decimal place.

boundaries for $\Omega_1 = \Omega_2 = \Omega_3 = 0.3$ in the original TASEP-LK. We find that the shockwave phase appears at different locations compared to the case of $\Omega_1 = \Omega_2 = \Omega_3$.

Moreover, we show how the shockwave phase boundaries depends on parameters Ω_1, Ω_2, and Ω_3 in Fig. 4.4. Figures 4.4 (a), (b), and (c) show how the shape of the shockwave phase varies for $\Omega_2 = 0.4$. When the values of Ω_1 and Ω_3 are increased, we can see that the shockwave phase is spread. Then, Figs. 4.4 (d), (e), and (f) show the shape variation of the shockwave phase for $\Omega_1 = 0.1$ and $\Omega_3 = 0.05$. When the value of Ω_2 is increased, we can see that the upper right area of the shockwave phase spreads out. In addition, if we swap the values of Ω_1 and Ω_3, the shape of the shockwave phase becomes symmetrical to $\alpha = \beta$.

4.4.2 Density profile

We show the density profiles observed on each phase in Fig. 4.5. Figure 4.5 show the density profiles in the steady state obtained by use of a mean-field approximation and performing Monte Carlo simulations with $L = 1000$.

In consequence, we find that the mean-field approximation and Monte Carlo simulation results are generally consistent.

4.4.3 Position of the domain wall

We examine the effect of the attachment and detachment parameters and the rates of inflow and outflow at the boundaries on the existence and the position of the DW.

We compare the density profile for the TASEP ($\Omega_1 = \Omega_2 = \Omega_3 = 0$), the original TASEP-LK ($\Omega_1 = \Omega_2 = \Omega_3 = 0.3$), and the TASEP-LKFB ($\Omega_1 = 0.3$, $\Omega_2 = 0.4$, and $\Omega_3 = 0.2$) computed by Monte Carlo simulations on $\alpha = \beta = 0.1$ in Fig. 4.6. The density profile of the TASEP is line shape, because the DW performs a random walk over time. From Fig. 4.6, we can see that the positions of DWs are different between the original TASEP-LK and the TASEP-LKFB.

Next, we show how the positions of the DWs are changed by varying the values of $\alpha = \beta$ for $\Omega_1 = 0.3$, $\Omega_2 = 0.4$, and $\Omega_3 = 0.2$ in Fig. 4.7. From Fig. 4.7, it can be seen that the positions of the DWs are shifted to the left little by little with decreasing $\alpha = \beta$. In the case of the original TASEP-LK where $\Omega_1 = \Omega_2 = \Omega_3$, the position of the DW has been calculated as $x_{\mathrm{DW}} = 1/2$ when the rates at the right and left boundaries are equal [13]. In contrast,

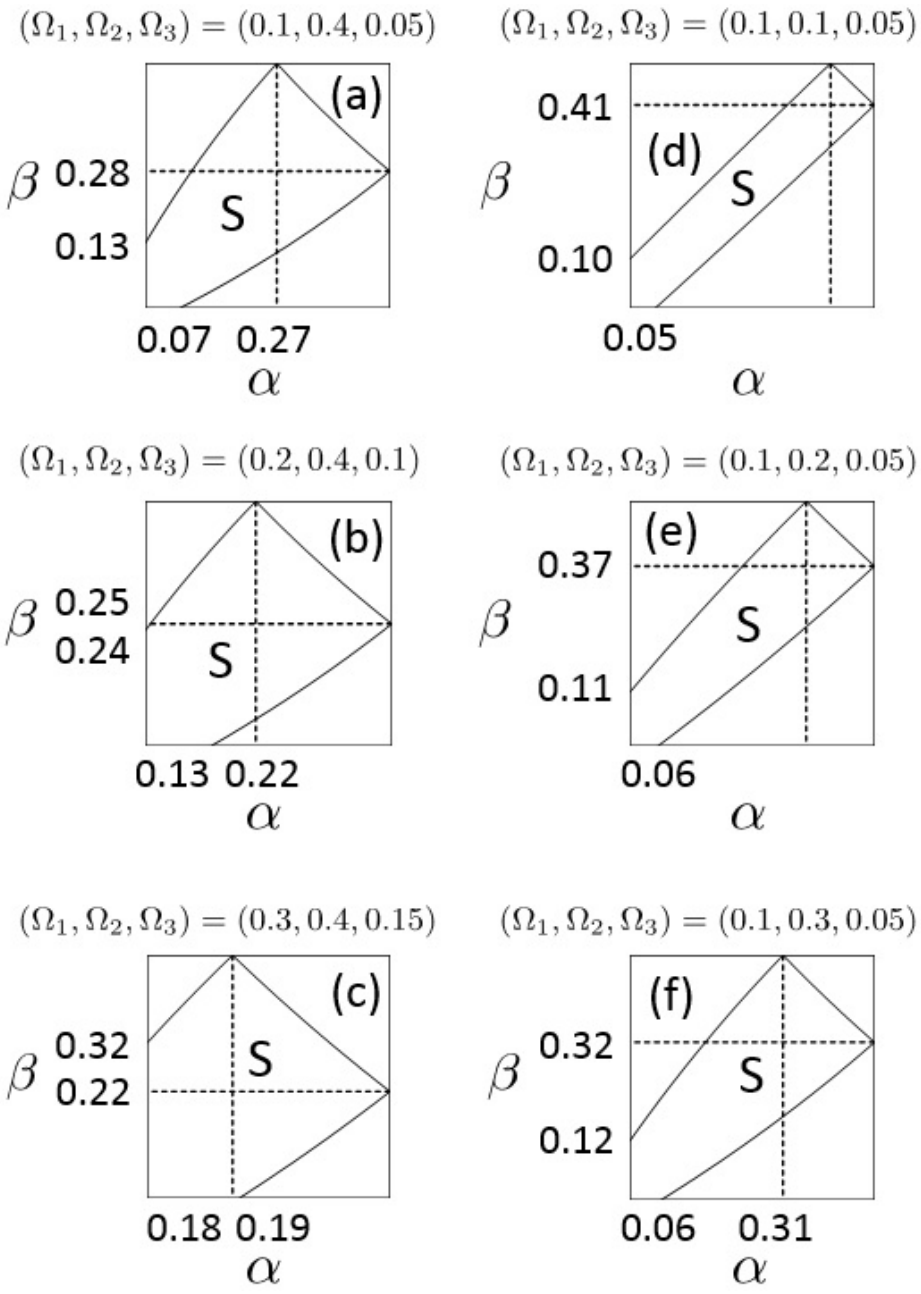

Figure 4.4: These figures show the shape of shockwave phase. The values are rounded off to the second decimal place.

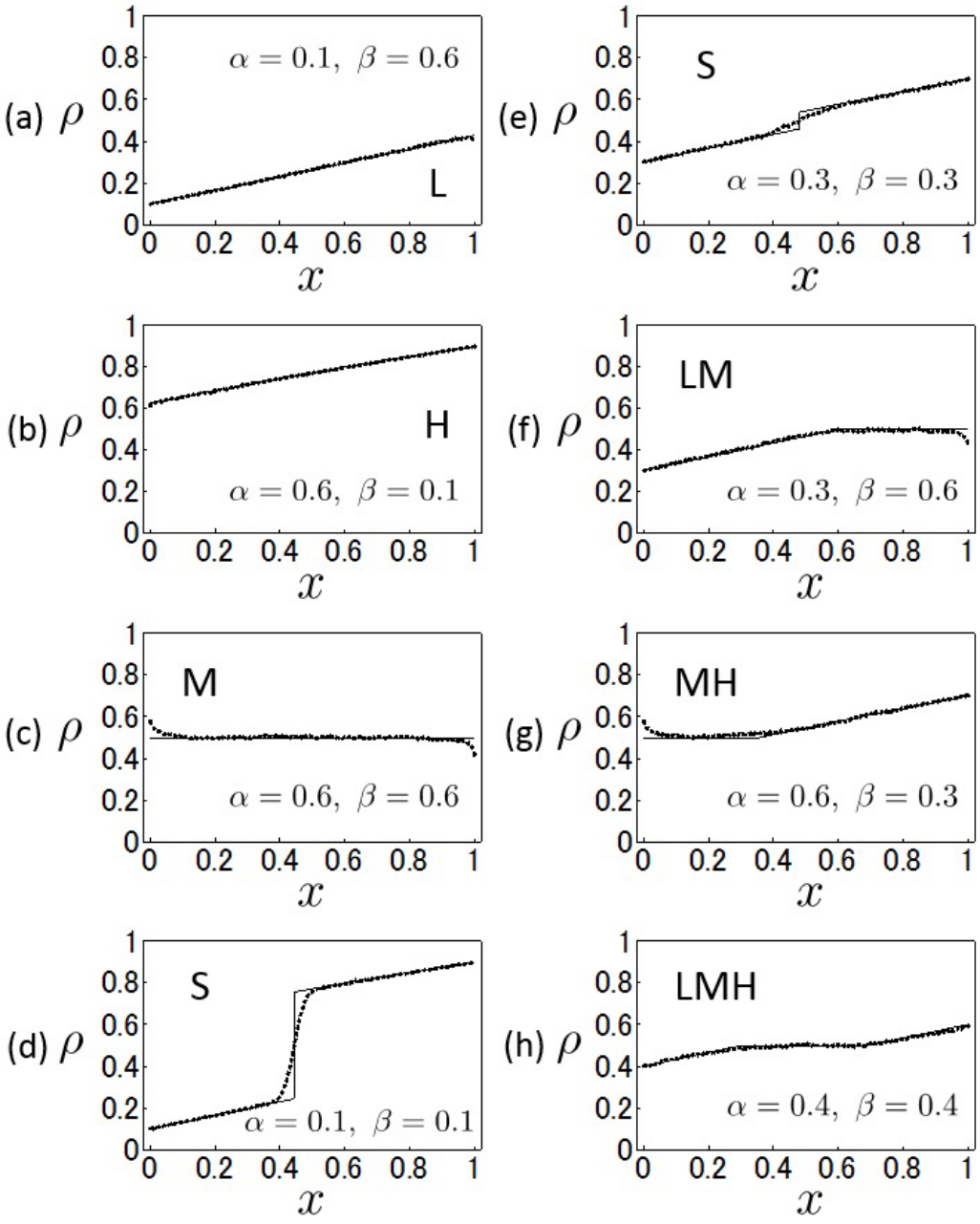

Figure 4.5: Density profile $\rho(x)$ for $\Omega_1 = 0.3$, $\Omega_2 = 0.4$, and $\Omega_3 = 0.2$. Solid lines are the results using a mean-field approximation. Dotted lines are average density profiles computed by Monte Carlo simulations.

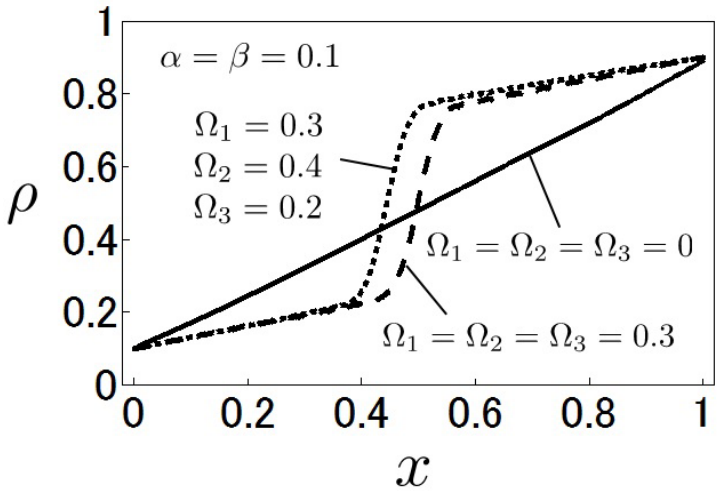

Figure 4.6: Density profile $\rho(x)$ computed by Monte Carlo simulations for the TASEP ($\Omega_1 = \Omega_2 = \Omega_3 = 0$), the original TASEP-LK ($\Omega_1 = \Omega_2 = \Omega_3 = 0.3$), and the extended TASEP-LK ($\Omega_1 = 0.3$, $\Omega_2 = 0.4$, and $\Omega_3 = 0.2$) on $\alpha = \beta = 0.1$.

in our model, we have found that x_{DW} can move according to $\alpha = \beta$, which is distinctive characteristic induced by the additional local interaction rules.

Finally, we examine how the positions of DWs are changed by each value of the attachment and detachment parameter Ω_1, Ω_2, and Ω_3. Figures 4.8 and 4.9 show the density profile computed by Monte Carlo simulations and the position of the DW obtained from a mean-field approximation in $\alpha = \beta = 0.1$.

Figure 4.8 (a) shows the density profile computed by Monte Carlo simulations for each $\Omega_3 = 0$, 0.1, 0.2, and 0.3 in case of $\Omega_1 = \Omega_2 = 0.3$. Figure 4.8 (b) shows the relationship between Ω_3 and the position of the DW obtained from a mean-field approximation for each $\Omega_1 = \Omega_2 = 0.05$, 0.1, 0.15, 0.2, 0.25, and 0.3. We can see from Fig. 4.8 that the position of the DW moves to the right when Ω_3 becomes larger.

In addition, Fig. 4.9 (a) shows the density profile computed by Monte Carlo simulations for each $\Omega_1 = 0$, 0.1, 0.2, and 0.3 in case of $\Omega_2 = \Omega_3 = 0.3$. Figure 4.9 (b) shows the relationship between Ω_1 and the position of the DW obtained from a mean-field approximation for each $\Omega_2 = \Omega_3 = 0.05$, 0.1, 0.15, 0.2, 0.25, and 0.3. In Fig. 4.9, on the contrary to Fig. 4.8, the DW appears on the more left side with increasing Ω_1.

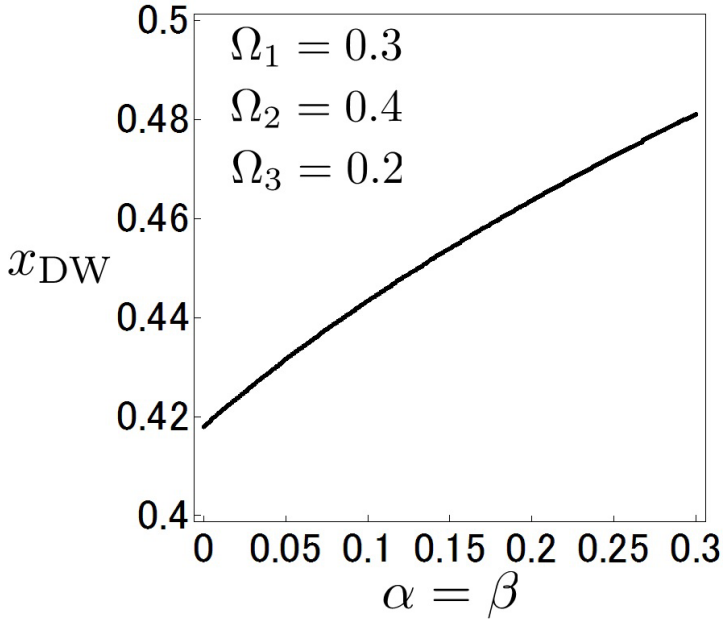

Figure 4.7: The relationship between the inflow and outflow rates $\alpha = \beta$ and the position of the DW x_{DW} for $\Omega_1 = 0.3$, $\Omega_2 = 0.4$, and $\Omega_3 = 0.2$ obtained from a mean-field approximation.

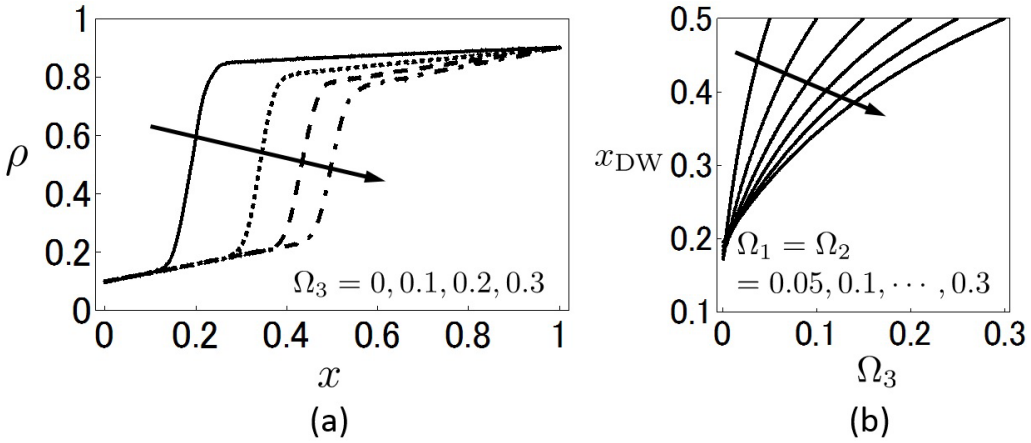

Figure 4.8: Inflow and outflow rates are fixed at $\alpha = \beta = 0.1$. (a) Density profile $\rho(x)$ computed by Monte Carlo simulations for each $\Omega_3 = 0$, 0.1, 0.2, and 0.3 in case of $\Omega_1 = \Omega_2 = 0.3$. (b) The relationship between Ω_3 and $x_{\rm DW}$ using a mean-field approximation for each $\Omega_1 = \Omega_2 = 0.05$, 0.1, 0.15, 0.2, 0.25, and 0.3.

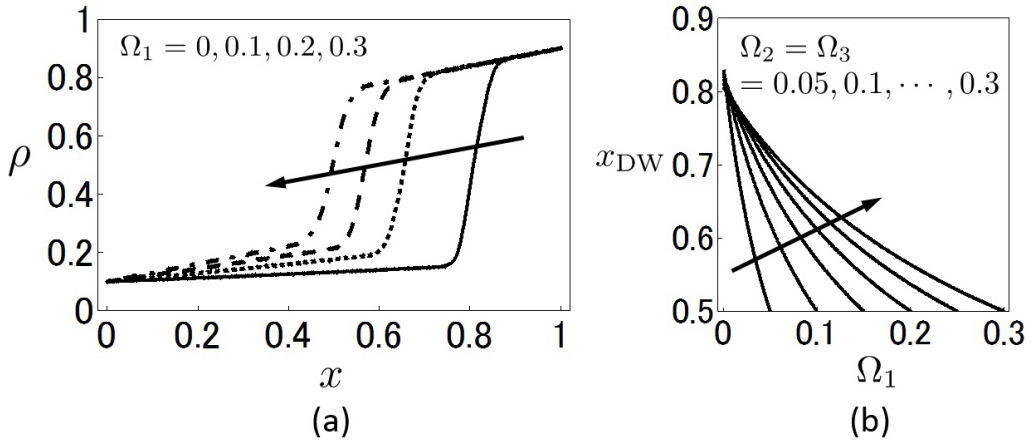

Figure 4.9: Inflow and outflow rates are fixed at $\alpha = \beta = 0.1$. (a) Density profile $\rho(x)$ computed by Monte Carlo simulations for each $\Omega_1 = 0$, 0.1, 0.2, and 0.3 in case of $\Omega_2 = \Omega_3 = 0.3$. (b) The relationship between Ω_1 and $x_{\rm DW}$ using a mean-field approximation for each $\Omega_2 = \Omega_3 = 0.05$, 0.1, 0.15, 0.2, 0.25, and 0.3.

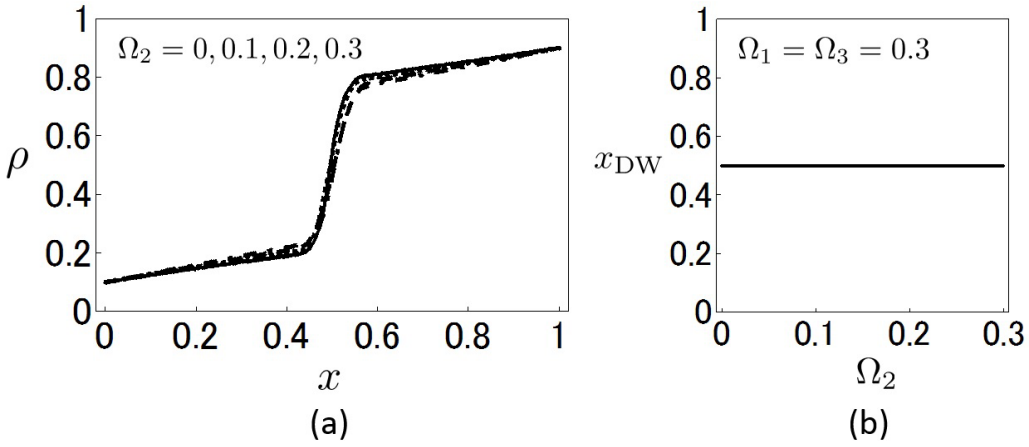

Figure 4.10: Inflow and outflow rates are fixed at $\alpha = \beta = 0.1$. (a) Density profile $\rho(x)$ computed by Monte Carlo simulations for each $\Omega_2 = 0$, 0.1, 0.2, and 0.3 in case of $\Omega_1 = \Omega_3 = 0.3$. (b) The relationship between Ω_1 and x_{DW} using a mean-field approximation for $\Omega_1 = \Omega_3 = 0.3$.

On the other hand, in the case of $\Omega_1 = \Omega_3$, the position of the DW appears at the midpoint as shown Fig. 4.10.

4.4.4 Effect of the boundary flow rates

We examine the effect of the inflow and outflow rates at the boundaries on the density profile. We perform Monte Carlo simulations with $L = 100$.

On the premise of $\Omega_1 = 0.3$, $\Omega_2 = 0.4$, and $\Omega_3 = 0.2$, Fig. 4.11 (a) shows the density profile on the condition that $\alpha = 0.1$ is fixed and β is variable, and Fig. 4.11 (b) shows the density profile on the condition that $\beta = 0.1$ is fixed and α is variable. From the figure in this case, we can see that the density profile is affected by the both inflow rate α and outflow rate β.

Next, Figs. 4.12 (a) and (b) are under the premise of $\Omega_1 = 0.3$, $\Omega_2 = 0.4$, and $\Omega_3 = 5$, then $\alpha = 0.1$ is fixed and β is variable in (a), and $\beta = 0.1$ is fixed and α is variable in (b). The figure shows that the density profile is less affected by the outflow rate β when the value of Ω_3 becomes large.

Furthermore, Figs. 4.13 (a) and (b) are under the premise of $\Omega_1 = 5$, $\Omega_2 = 0.4$, and $\Omega_3 = 0.2$, and then the condition of α and β are the same as above. Contrary to Fig. 4.12, we can see that the density profile is less affected by the inflow rate α when the value of Ω_1 becomes large.

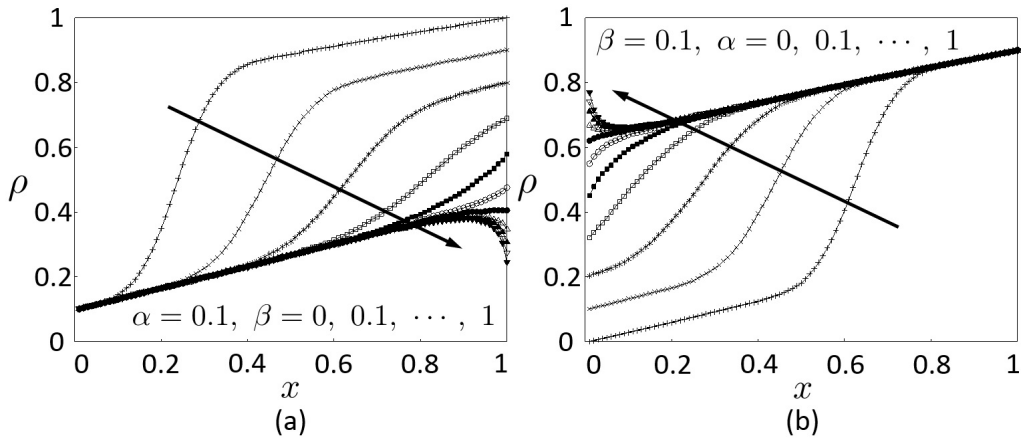

Figure 4.11: Density profile $\rho(x)$ for $\Omega_1 = 0.3$, $\Omega_2 = 0.4$, and $\Omega_3 = 0.2$. (a) $\alpha = 0.1$ is fixed and $\beta = 0.1 \times k$, $k = 0, 1, \cdots, 10$. (b) $\beta = 0.1$ is fixed and $\alpha = 0.1 \times k$, $k = 0, 1, \cdots, 10$.

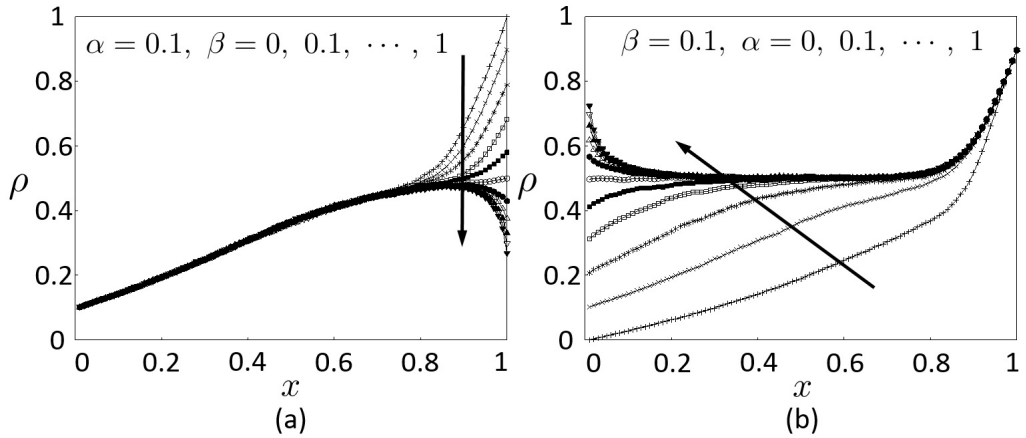

Figure 4.12: Density profile $\rho(x)$ for $\Omega_1 = 0.3$, $\Omega_2 = 0.4$, and $\Omega_3 = 5$. (a) $\alpha = 0.1$ is fixed and $\beta = 0.1 \times k$, $k = 0, 1, \cdots, 10$. (b) $\beta = 0.1$ is fixed and $\alpha = 0.1 \times k$, $k = 0, 1, \cdots, 10$.

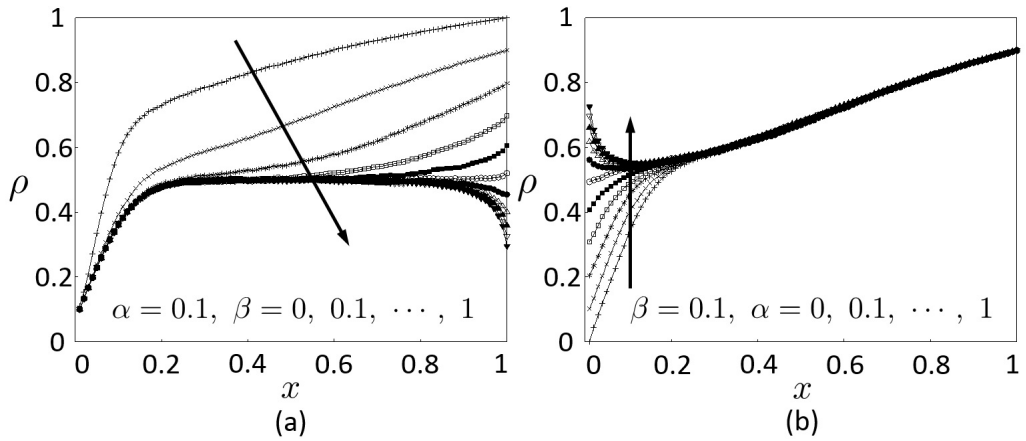

Figure 4.13: Density profile $\rho(x)$ for $\Omega_1 = 5$, $\Omega_2 = 0.4$, and $\Omega_3 = 0.2$. (a) $\alpha = 0.1$ is fixed and $\beta = 0.1 \times k$, $k = 0, 1, \cdots, 10$. (b) $\beta = 0.1$ is fixed and $\alpha = 0.1 \times k$, $k = 0, 1, \cdots, 10$.

Finally, Figs. 4.14 (a) and (b) are under the premise of $\Omega_1 = 0.3$, $\Omega_2 = 5$, and $\Omega_3 = 0.2$, and then the condition of α and β are also the same as above cases. When the value of Ω_2 becomes large, the density profile tends to be pulled to 1/2. Although the density profile is affected by the both inflow rate α and outflow rate β, the influence is less than Fig. 4.11.

Hereafter, we give the physical explanation of the above observations. In the case of large Ω_1, the attachment and detachment of particles in the low density area relatively increase. Since the attachment rate and detachment rate are set to be the same, there is no influence, at first sight, in the situation. However, since particles hop in one direction, a particle coming into the low density area goes forward and bumps into the forward particle. Consequently, the value of low density area tends to increase and the density profile becomes less influenced by the inflow rate α.

On the other hand, in the case of large Ω_3, the attachment and detachment of particles in the high density area relatively increase. Then, due to the detachment of particles from the high density area, each particle gets easy to go forward on the whole system. According to this effect, the value of the high density area tends to decrease, and the density profile becomes less affected by the outflow rate β.

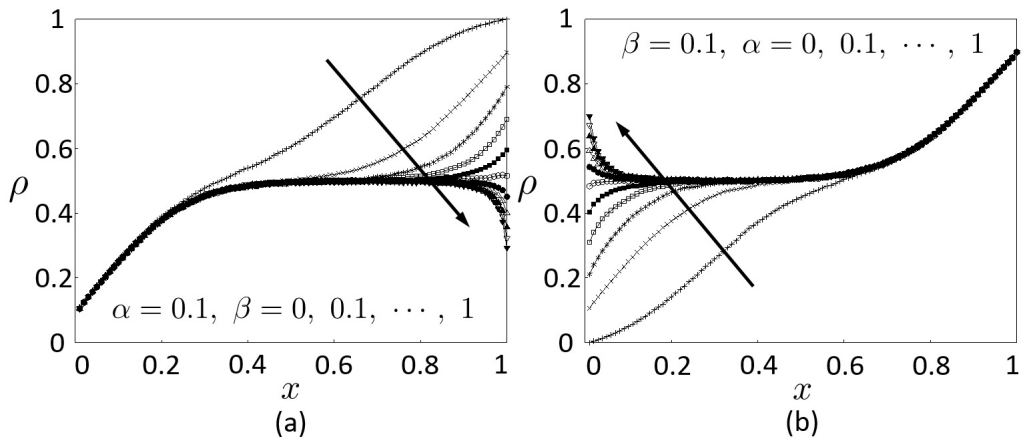

Figure 4.14: Density profile $\rho(x)$ for $\Omega_1 = 0.3$, $\Omega_2 = 5$, and $\Omega_3 = 0.2$. (a) $\alpha = 0.1$ is fixed and $\beta = 0.1 \times k$, $k = 0, 1, \cdots, 10$. (b) $\beta = 0.1$ is fixed and $\alpha = 0.1 \times k$, $k = 0, 1, \cdots, 10$.

4.4.5 Periodic boundary condition

We briefly comment on the steady state for the periodic boundary. From (4.5) and Monte Carlo simulations, we find that the density profile is a constant function $\rho(x) = 1/2$ in the periodic boundary case for arbitrary Ω_1, Ω_2, and Ω_3. From the above, in only case of the open boundaries, it is a point of interest that the density profile depend on each value of the attachment and detachment parameter Ω_1, Ω_2, and Ω_3.

4.5 Summary

In this chapter, we studied the TASEP-LK with a distinction that the rates of attachment and detachment depend on the states of the forward and backward neighboring sites. Then, the steady state of the model was analytically examined.

Our model is considered to be a generalization of the one studied by Vuijk *et al.* [43] for the case that the attachment rate and detachment rate are equal in each state of the neighboring sites. In our model, more specifically, the states of the neighboring sites were classified more finely than theirs. In addition, each attachment and detachment rate can take arbitrary values independently in our model.

In consequence, we succeeded in presenting a density profile by use of a

mean-field approximation and obtaining analytically the position of the DW. From a comparison between the results using a mean-field approximation and Monte Carlo simulations, we found that both of them were generally consistent. Moreover, we found more in detail that the density profile is changed by manipulating the attachment and detachment parameters. In particular, it was shown that the position of the DW, which is fixed in the original model, changes depending on the inflow and outflow rates when the rates at the right and left boundaries are the same. In addition, we observed from the phase diagram that the shockwave phase boundaries are distorted by the additional local interaction rules.

There are many actual phenomena that directly involve the attachment or detachment on the bulk of a lattice such as molecular motors and traffic flow. We think that the extended model has a great deal of potential to describe such complex phenomena more in detail. The further generalization of this model and its application to actual phenomena will be studied in the future.

Chapter 5

Collective phenomena in actual complex system

5.1 Preface

In this chapter[‡], we take up a trading mechanism called the continuous double auction [16, 18] used in many financial instruments exchanges which we introduced in Sec. 1.2 as actual complex systems. We study the phenomena caused by the mechanism of attachment and detachment from the point of concrete views. Because the financial instruments exchange is digitized, there are huge stocks of trading data. Therefore, in the field such as econophysics, it is actively studied as the complex systems in the society [19, 20]. Since many results to confirm the reproducibility are available in the previous studies, the trading mechanism in the financial instruments exchange is suitable for the analysis on the cause of the phenomena with modeling. We deliberate here an occurrence factor of large-scale price movements observed in various financial markets by using a order-book model which is often adopted in the analysis about the mechanism of the trading and the price building in the financial instruments exchange [16, 17, 20, 35, 36, 54–60].

R. N. Mantegna and H. E. Stanely have pointed out, prices actually do not ideally move following a normal distribution [61]. In reality, it is generally known that large-scale price movement more frequently occurs than that assumed by a normal distribution. Moreover, it is known that a

[‡]This chapter is composed of the contents partially modified based on [35, 36]. The final publication of [35] is available at ELSEVIER via http://dx.doi.org/10.1016/j.physa.2014.11.016. The final publication of [36] is available at Springer via http://dx.doi.org/10.1007/978-3-319-20591-5.

power law emerges from the distribution of the return of the U.S. stock markets [62,63]. For the market participants, it is crucial to estimate accurately the profitability and downside risk of financial products they trade in.

We focus on investors' collective behavior that they order with following for the price movement of the past as one of the occurrence factors of large-scale movements. For example, once the price begins to continuously decline, investors fear downside risk, and they follow the trend by lowering the prices of their orders [64]. We consider that this is one of the mechanisms by which price decline causes further declination, leading to an extreme price fall. In addition, Y. Hashimoto *et al*. used actual foreign exchange market data and indicated that the price is dependent on past price trends [65].

Thus, we study whether investors' collective behavior that orders are done following the past price movement can be the occurrence factor of large-scale price movements by a simulation model [35]. In particular, we consider the degree how the price moves continuously in one direction by a positive feedback which occurred unexpectedly and the relation between its size and frequency. In the reality, investors' collective behaviors appear as action of taking orders in and out (orders and cancellations) on the order book. Therefore, we reproduce the investors' collective behavior such as following for the past price movement by manipulating the mechanism of attachment and detachment in the simulation model.

Especially, if the power law is observed in the price movement, we can gather that there is some correlation among executions of trading [66]. In other words, it is considered that the appearance of the power law means the occurrence of one of self-organization [6, 67, 68]. Self-organization is a quite interesting objective of study on systems of self-driven particles. The study about the model based on the mechanism of attachment and detachment will give us the significant suggestion for the principle of the self-organization.

5.2 Basic rules

We explain the basic rules in the continuous double auction system using the electronic board called an order book that has been adopted by many financial instruments exchanges [15–18]. This system means a trading mechanism where buyers and sellers put their buy orders (bids) or sell orders (asks) each other on the order book and these orders are matched on according to certain rules.

Two order types are basically used in the financial instruments exchanges

which adopt the trading mechanism as this [17, 18, 69]. One is limit orders, that are used to indicate the highest (lowest) price on which buyers (sellers) wish to have their orders being executed. The other is market orders, that are used without an indication of price.

In addition, two principles are basically used as the matching rules [17, 18, 69]. One is the principle of price priority. On the basis of this rule, the highest priced bids on the order book are given priority over all other bids, and the lowest priced asks on the order book are given priority over all other asks. The highest bid price and the lowest ask price are called "best bid" and "best ask", respectively. The other important rule is the principle of time priority. If there are multiple orders in the same price on the order book, the oldest order is given priority against all other orders at that price, and will be executed first. As above, each priority in asks and bids respectively is determined and executed accordingly.

We introduced here the minimum of the basic rules which is necessary to propose simple order-book models. In fact, there are cases in which characteristic rules exist in each financial instruments exchange. In this study, we do not treat the complicated rules for analysis on the dynamics of basic price formation in the continuous double auction using the order book.

5.3 Model

Firstly, we introduce several models that capture a trading mechanism in a financial market. Secondly, we propose two simple order-book models for the continuous double auction using order book. Then, we explain how orders are selected for execution in our simulation models.

5.3.1 Previous models

Common statistical characters called "stylized facts" are observed from empirical data in different financial markets [70]. The stylized facts contain the absence of fat-tail, autocorrelations, volatility clustering, and others. Many of the models, such as an order-book models, agency-based models, and others have been actively studied to reproduce them. In this study, we take up an order-book model to capture the trading process and price formation based on the continuous double auction mechanism in the order book. In particular, the models with a stochastic orders is called the "stochastic order-book model" [16].

Bak *et al*. introduced the earliest simple models of a stock market [54]. In their model, sell and buy orders were modeled as two kinds of particles on a one-dimensional lattice whose positions correspond to price. Then, each particle diffuse along the lattice. When sell and buy particles locate the same lattice site, an annihilation of the sell and buy particles occurs.

Then, Maslov [55] proposed an order-book model was more like a trading system in reality. This model has been said that one of the pioneers of the stochastic order-book model [16]. In this model, limit order and market order are chosen with equal probability. Bid and ask orders are chosen with equal probability as well. The limit order price is selected by a uniform random number within a certain range from the last price. This is a very simple model, but it successfully captures the power law in the distribution of the price difference gathered through simulations. However, their model was not able to reproduce the suits Hurst exponent to reality.

After that, Maslov's model is developed by Challet and Stinchcombe [56]. They were able to reproduce the Hurst exponent close to reality at large time scales.

As other distinctive order-book model, Maskawa proposed a model where investors mimic the historical order trend [60]. In this model, with a certain probability, the priority given to an order's price is based on the price that has the greatest pooled order volume on the order book.

On the other hand, some great models should be noted in addition to the order-book models. G. Harras and D. Sornette proposed a model based on the Ising model. The model captures the collective behaviors of investors well [71]. Moreover, other studies have investigated agency-based models focusing on dealer behavior [72, 73].

5.3.2 Simulation models

We propose two simple stochastic order-book models [35,36]. One that dose not include the collective behavior is denoted as the "basic model". The other that incorporates the collective behavior of investors. The collective behavior is investors' following a trend in the historical price movement. We denote the model as the "following model".

5.3.2.1 Basic model

We explain selection method of the order price in the basic model [35, 36]. The model assumes an equal probability that a new order is a bid or an ask,

and the price of the order is selected randomly within a specified range from the most recent execution-price p_n. We specify a range of $[p_n - 15,\ p_n + 15]$. For example, if the most recent execution-price $p_n = 100$, the bid or ask price is randomly selected within the range [85, 115], and one unit will be placed on the order book.

In addition, we employ an order canceling rule. This rule is a mechanism for canceling the orders outside the specified range of $[p_n - 15,\ p_n + 15]$ on the order book. We use this mechanism because in reality, investing information is abundantly and readily available to investors; therefore, it is unlikely that their orders would be left on the order book when the price has moved sufficiently away from their order price. In addition, in markets led by professional traders, traders are constantly calculating the theoretical price of a product; therefore, the entire trading community has similar ideas regarding appropriate pricing. Therefore, it is realistic to remove an order whose price is placed outside the established range from the most recent execution-price.

Our models do not incorporate market orders. However, because an order is always placed in terms of one unit only, when an order is immediately executed, it could be interpreted as being a market order because it has the same effect as a market order.

5.3.2.2 Following model

We explain selection method of the order price in the following model [35]. The following model is for the follower behavior where investors order in accordance with a trend in the historical price movement.

To model this behavior, "the price range" from the most recent execution-price p_n used in the basic model is broken down into three ranges: first is price range $[p_n + 6,\ p_n + 15]$, second is price range $[p_n - 5,\ p_n + 5]$ and third is price range $[p_n - 15,\ p_n - 6]$. Usually, an order will be randomly placed within the $p_n \pm 15$ price range as in the basic model. However, when the historical price movement has an upward or a downward trend, orders will be placed within the three ranges with different probabilities. We define a trend-index Δ to determine the upward and downward trend in the price movement as follows:

$$\Delta := \sum_{j=1}^{10} \mathrm{sgn}(\delta_j), \tag{5.1}$$

where

$$\mathrm{sgn}(\delta_j) = \begin{cases} +1, & \delta_j > 0 \\ 0, & \delta_j = 0 \\ -1, & \delta_j < 0 \end{cases}, \tag{5.2}$$

and $\delta_j = p_{n-(j-1)} - p_{n-j}$. If $\Delta \geq +9$ ($\Delta \leq -9$), we define that the price movement has on upward trend (downward trend). When the price is in the upward trend, the probability of placement will be 0.8 in the price range $[p_n + 6,\ p_n + 15]$ and 0.1 in both the price ranges $[p_n - 5,\ p_n + 5]$ and $[p_n - 15,\ p_n - 6]$. This difference of in probability expresses how investors consider a trend in the historical price movement and "collective behavior" to a certain price range. On the contrary, if the price is in the downward trend, both bids and asks will be placed within the price range $[p_n - 15,\ p_n - 6]$ with 0.8 probability, 0.1 will be applied as the order probability in the other two ranges.

As with basic model, this model has the order canceling rule and the order type is only the limit order.

5.3.2.3 Matching mechanism

We describe the matching mechanisms of our models. We consider only the principle of price priority as the matching rule. The time priority rule is not meaningful in our simulation because we do not distinguish agents who send orders.

Trading takes place whenever "best ask" $\leq$ "best bid" on the order book. The execution-price is either the price of the bid or ask order, whichever is on the order book first.

Figure 5.1 depicts a transaction. At State 1, the order book holds an order to sell four units at an ask price of 101 and an order to buy two units at a bid price of 99 and one unit at a bid price of 98. The most recent transaction price is 100. At State 2, one unit of a bid at a price of 102 is entered. Because of this new order, "best ask" $\leq$ "best bid"; therefore, at State 3, the transaction occurs between the one unit ask at a price of 101 and the new bid at a price of 102. The execution-price is 101.

5.4 Simulation results

This section compares price movements in each model.

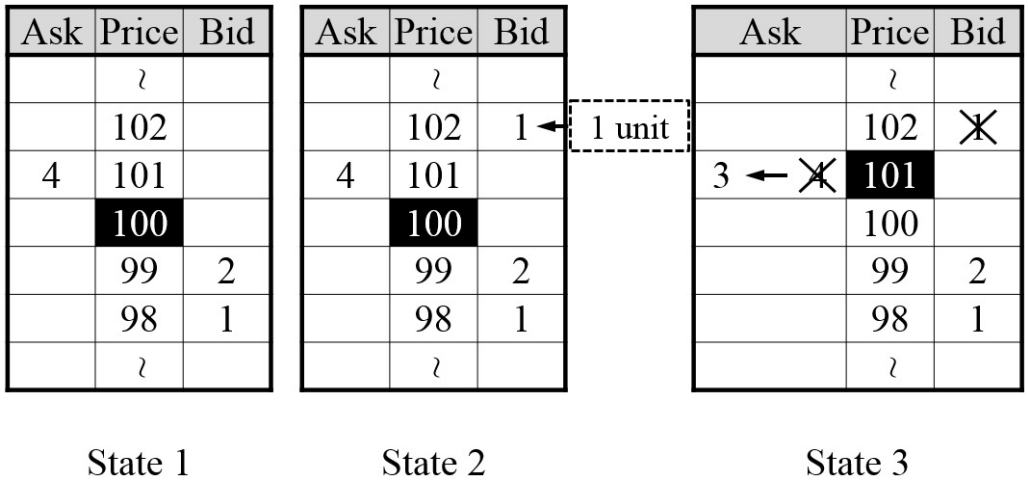

Figure 5.1: Drawing exemplifying an order book transaction.

First, we performed simulations for the basic and following models. One million simulations were performed 10 times for each model. Transactions occurred with the ratios $29.04\% \pm 0.03\%$ for the number of simulations using the basic model and $29.02\% \pm 0.03\%$ for the number of simulations using the following model. We analyze them by use of tick data (transaction data). A tick means the minimum unit of the price movement. From this, we call the number of transactions the number of ticks as "time". Then the time scale does not mean the actual time here. Figure 5.2 shows $10,000$ ticks of transaction data.

Illustrating how prices diffuse with time, Fig. 5.3 shows the relation between the standard deviation of the price gap $p_{n+\tau} - p_n$ and the time scale (tick) τ on a double-logarithmic graph. The relationship $\sigma(\tau)$ between the standard deviation of the price gap and the time scale (tick) is as follows [16]:

$$\sigma(\tau) = \sqrt{\langle (p_{n+\tau} - p_n)^2 \rangle - \langle p_{n+\tau} - p_n \rangle^2} \propto \tau^H, \quad \tau \geq 1, \tag{5.3}$$

where $\langle \cdot \rangle$ is the sample average, and H is Hurst exponent. The dotted line is the one-half power of the time scale (tick) τ. We here estimate Hurst exponent by linearizing the points plotted on the double-logarithmic graph. Each Hurst exponent of the basic model and the following model is 0.48 and 0.50.

Next, we analyze the extent to which prices move continuously in one direction. Therefore, we obtain tick data from our simulations and analyze

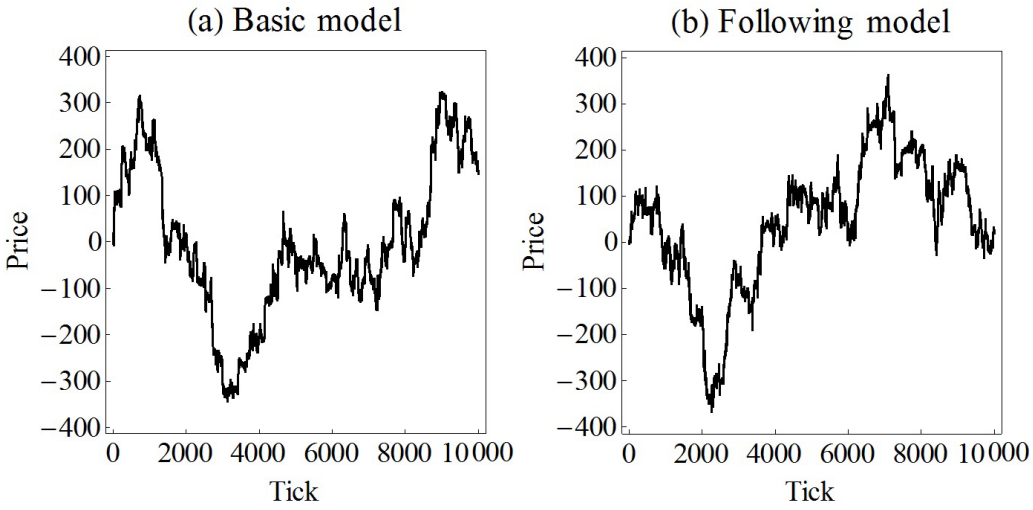

Figure 5.2: Price movements for 10,000 ticks. Fluctuations are obtained by simulations using (a) the basic model and (b) the following model.

a cumulative distribution function (CDF) of the price range by continuous movement. An indicator called "drawdown" ("drawup") is often used to capture a continuous loss (profit). In this study, we introduce a similar indicator to these. A drawdown (drawup) usually shows the loss (profit) from the last peak (bottom) of the price to the next bottom (peak) [16, 74, 75]. However, we consider that the continuous fall (rise) is interrupted when orders are executed multiple times continuously at the same price. In addition, we do not differentiate whether price movements are toward downside or upside because we are interested in the extent of continuous movement. We call the range of the continuous price movement as this "draw size" and capture the features of the price movements by using this indicator.

We analyze the CDF of the draw size from the basic and following models, respectively. Figure 5.4 (A) illustrates the CDF that compare the draw size from the basic model and the draw size from shuffled price gap data ($\tau = 1$) from the basic model on the semilogarithmic graph. The solid line depicts a linearization of the CDF for draw size of 16 and larger from the basic model (slope $= -0.04$). The dotted line depicts a linearization of the CDF for draw size of 16 and larger from the shuffled price gap data from the basic model (slope $= -0.06$). Then, Fig. 5.4 (B) illustrates the CDF that compare the draw size from the following model and the draw size from shuffled price gap

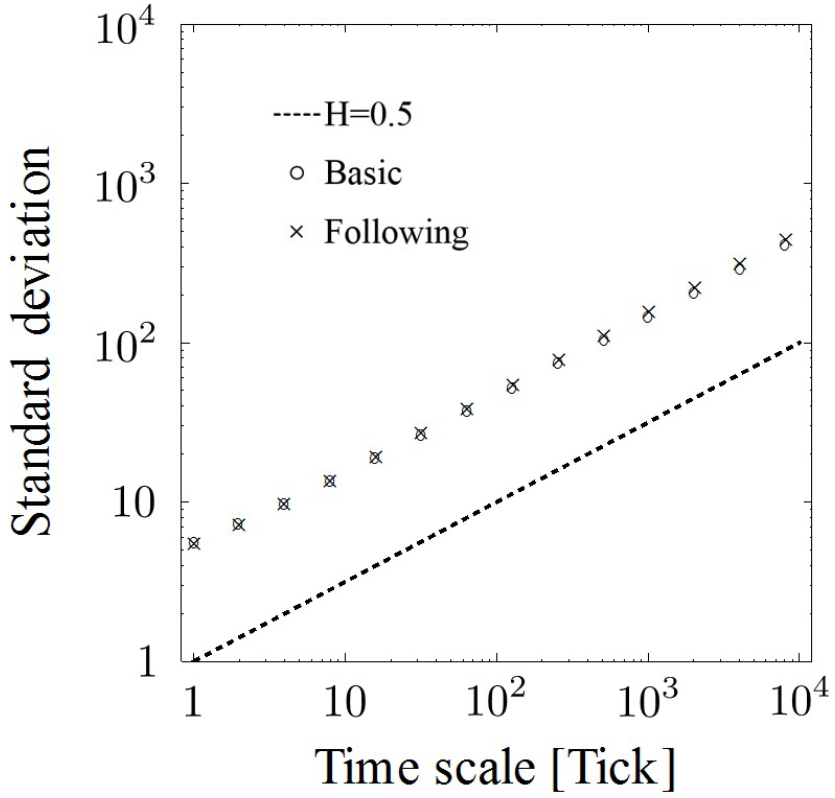

Figure 5.3: Double-logarithmic graph of the standard deviations of price gaps with respect to the time scale (tick) derived from the basic model and following model.

data ($\tau = 1$) from the following model on the semilogarithmic graph. The chain line depicts a linearization of the CDF for draw size of 16 and larger from the shuffled price gap data from the following model (slope $= -0.06$).

Finally, we analyzed the tail of CDF of the draw size from the following model. Figure 5.5 is the double-logarithmic graph for tail of CDF of the draw size from the following model. This graph is used all draw size data of all classes including the largest 0.5%. The solid line is a power-law distribution created by the maximum-likelihood method using the tail model as follows [16, 76, 77]:

$$P_{>}(x) = r\int_{x}^{\infty} f(u)du = r\left(\frac{s}{x}\right)^{\mu}, \quad \text{where} \quad f(u) = \mu\frac{s^{\mu}}{u^{\mu+1}}, \tag{5.4}$$

r denotes the ratio of the number of draw size data ($x \geq s$) against the

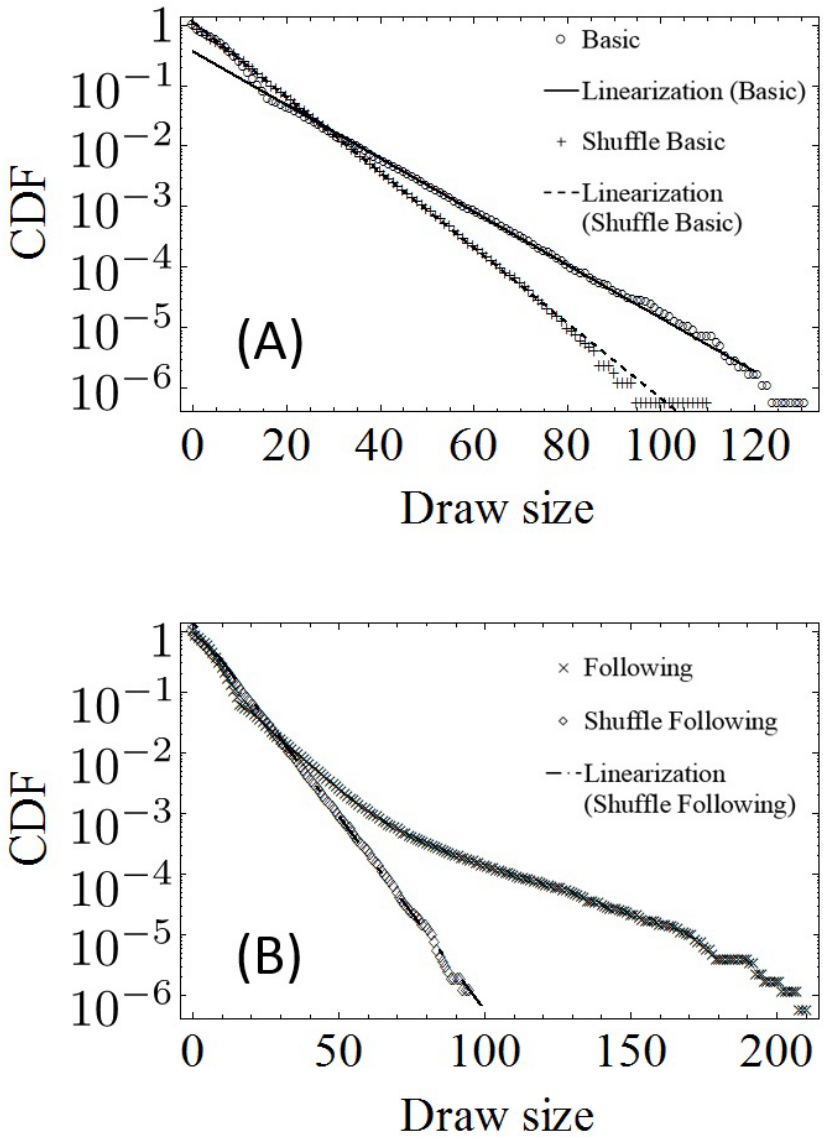

Figure 5.4: Semilogarithmic graph of the CDF for a draw size. (A) Basic model (Basic) and shuffled price gap data from the basic model (Shuffle Basic). (B) Following model (Following) and shuffled price gap data from the following model (Shuffle Following).

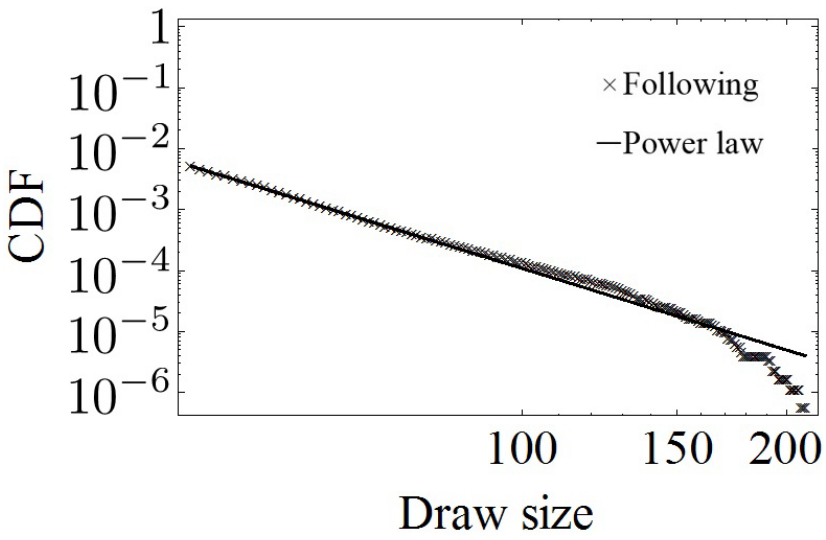

Figure 5.5: Double-logarithmic graph for the tail of the CDF of the draw size from the following model (Following). The solid line is a power-law distribution (Power law).

number of all data, and s is the smallest draw size of the tail. This solid line follows the formula below.

$$P_{>}(x) \propto x^{-4.45}.$$

5.5 Discussion of the numerical results

In this section, we examine the results of the empirical analysis in the previous section.

Firstly, we compared the price movements of the two models in Fig. 5.2. We found little difference between the behavior of the basic model and the following model, even in the price movement graph.

Secondly, we showed that the standard deviation of the price gap for the time scale (tick) is roughly proportional to the one-half power of the time scale (tick) for each model in Fig. 5.3. This is similar to the results obtained from past experiential study [16, 60], which reported that slow diffusion occurred over a short time scale, where the Hurst exponent was below 0.5, and approached a value of 0.5 at a longer time scale. However, the data derived from the current simulations exhibited an absence of slow

diffusion over short time scale. This indicates that the price data from each model has similar diffusion speed representative of a random walk.

Thirdly, we studied the CDF of the draw size in the basic and following models, respectively. Figure 5.4 (A) suggest that the price data of the basic model resemble a random walk. If a random walk is assumed in a market, a given draw size will occur exponentially less frequency when its size is larger [75]. Therefore, we consider that the basic model is similar to an ideal market that resembles a random walk. On the other hand, Fig. 5.4 (B) indicates that the price movements from the following model have the emergent temporal correlations. This show that, the larger the draw size, the wider the tail of the CDF. We think that price data from the following model exhibit correlation such as a local chain according to the price movement. Therefore, the following model successfully captures the effect of collective behavior following a historical trend.

Finally, we estimated the power exponent from the data at around the tail for the following model. In the result, we found that the part of tails on CDF of draw size for the following model could be approximated by power-law distribution. This shows that investors' collective behaviors produced by investors interacting create a phenomenon similar to a significant price decline. In fact, it was shown that the distribution of the drawdown obtained from actual market data has a fatter tail than the exponential distribution of the expected distribution that assumes a complete random walk market [74, 75]. Although the shape of the distribution is subject to further discussion, the results of previous empirical studies are similar to our simulation results; therefore, we suggest that multiple investors' ordered behaviors interact and then create large-scale price movements which are rare events in the actual markets. We think that in the real market, when there are many investors that trade by following the historical price movement, there will be events that the typically assumed random walk cannot capture.

5.6 Summary

In this chapter, we took up the trading system in the financial instruments exchange as the system of self-driven particles with mechanism of attachment and detachment in actual. We proposed the basic model in which the price of order is selected randomly and the following model incorporated investors' collective behavior in the basic model.

We found that the CDF of the draw size obtained from this basic model

could be approximated by exponential function. On the other hand, we found that the parts of tails became thick in the CDF on the draw size obtained from the following model. Through comparing the results obtained from the both models, we understand that investors' collective behavior following the past price movement yield the change of distribution. In other words, as one occurrence factor of large-scale price movements which are observed as rare events in the financial market, such investors' collective behavior is considered to be related to that. These analyses are important in the viewpoint of the risk management in financial markets.

Chapter 6

Conclusive discussion

In this thesis, we studied for the purpose of understanding the general principle and universal structure in cross-cutting for the collective dynamics of self-driven particles with attachment and detachment. We proposed new mathematical models based on ASEP which has been studied actively as the model of non-equilibrium system. In particular, we concretely analyzed the mechanism of attachment and detachment and generalized the original TASEP-LK.

At first, we considered the TASEP on a periodic lattice with LK depending on the states of the forward neighboring site (TASEP-LKF). This model was proposed against a background of the traffic flow with lane changing. Then, the density profile in the steady state and the relaxation dynamics were analytically examined. As a consequence, we could obtain explicitly the expressions of the density profile in the steady state and the relaxation dynamics in high accuracy by using a mean-field approximation. Therefore, we succeeded in obtaining analytically the structure of the dynamics in this model. In addition, the results showed a very natural behavior and exceeded the expectations for the traffic flow with the lane changing obtained by investigating some numerical examples.

Next, we considered the TASEP on a one-dimensional open lattice with LK depending on the states of the forward and backward neighboring sites (TASEP-LKFB). Considering both the states of the forward and backward neighboring sites, this model was proposed for the purpose of understanding the structure of more complex mechanisms of attachment and detachment and applying it in more versatile way. In this model, the model of Vuijk *et al.* was generalized on the point that each attachment and detachment rate can respectively take independent arbitrary value under the condition that

attachment rate and detachment rate are equal. Following, we analyzed the density profile in the steady state by using a mean-field approximation. After comparison with Monte Carlo simulations, we found that the density profile obtained by using a mean-field approximation reproduced the phenomena on the steady state with high accuracy. Therefore, we succeeded in obtaining analytically the more detailed structure on the steady state in the case that attachment rate and detachment rate are equal.

Finally, we took up a trading mechanism in the financial instruments exchange as the actual system of self-driven particles with mechanism of attachment and detachment. This study was carried out in order to capture the phenomena caused by the mechanism of attachment and detachment a more concrete point of view. We especially considered the influence on the price movement by representing investors' collective behavior following the past price movement as one of the rules of attachment and detachment. As a result, we found that the tails of CDF for the draw size became thick in the case of the model with investors' collective behavior. In other words, it was found that investors' collective behavior following to the past price movement had an influence as one of the occurrence factor of large-scale price movement. Moreover, based on the analysis of the shape of the tails' parts, we also found that it is likely to obey a power law. It is considered that the observation of power law means the occurrence of a certain self-organization. We could acquire a certain feeling on the more general understanding on the mechanism of the interesting phenomenon such as self-organization as well. In other words, for the result of this study, we found that the shape of the tails for distribution change when the attachment and detachment rates depend on time and space. In brief, it means that deep understanding of the actual phenomenon is achieved by studying the influence of the mechanism of attachment and detachment to the system. From the consideration above, we can see that the study focusing on the mechanism of attachment and detachment is important for capturing the interesting phenomena seen in the real non-equilibrium system.

We think that work for the future is to reveal the phenomena seen in the actual complex systems mathematically. In particular, it is a very interesting subject of study because there is potentially non-trivial general structure in phenomena caused by the mechanism of attachment and detachment. Although it is difficult in general to reveal a macroscopic structure mathematically from a microscopic behavior it is also a quite significant subject. In this regard we thank that the subject of a study like the one introduced here with TASEP-LK can have a great contribution on that issue. The TASEP-LK

is a quite appropriate model for mathematical analysis of the structure of non-equilibrium system with the mechanism of attachment and detachment from the microscopic viewpoint as we have presented in this thesis.

Actually, the study using the original TASEP-LK has been carried out for a trading mechanism in financial instruments exchanges that we introduced as the actual complex system in this thesis [57]. It has succeeded to capture the general phenomena such as transition of the price movement from over-diffusion to normal diffusion by this model. On the other hand, in the case of the order driven market, the effect of the volume exclusive in the ASEP dose not exist because multiple orders can be injected in one price. If we represent the dynamics in this market by the ASEP, it is considered as the method representing the number of orders in each price range by means of variation of attachment and detachment rates in each site. However, the dynamics of order (the mechanism of attachment and detachment) varies depending on the state of the whole system, location, time and so on in actual systems. We think the TASEP-LK that we newly proposed in this thesis can give us the novel tool for representing the complex mechanisms like the ones presented above.

Finally, the TASEP-LK has the potential to analyze the non-equilibrium systems with various mechanisms of attachment and detachment. We are going to advance the mathematical analysis on the TASEP-LK representing more complex mechanisms of attachment and detachment in the future and, at the same time, we think the interesting general structure will be revealed by considering applications to actual complex systems. In modern science, it is a large task to systematize issues that the non-equilibrium systems and the self-driven-particle systems based on the basic principles. We expect to accomplish those tasks by developing new studies in the future work.

References

[1] D. Helbing, Rev. Mod. Phys. **73**, 1067 (2001).

[2] 西成活裕, 『渋滞学』 (新潮社, 新潮選書, 2006) [18 刷, 2014].

[3] 西成活裕, 数理解析研究所講究録, 1472 巻, 118 (2006).

[4] A. Schadschneider, D. Chowdhury, and K. Nishinari, *Stochastic Transport in Complex Systems: From Molecules to Vehicles* (Elsevier Science, Amsterdam, 2010).

[5] 今井功, 『流体力学』 (岩波書店, 物理テキストシリーズ 9, 1970) [第 21 刷発行, 2014].

[6] 太田隆夫, 『非平衡系の物理学』 (裳華房, 2000) [第 6 版 2 刷発行, 2013].

[7] 田崎晴明, 『統計力学 I』 (培風館, 新物理学シリーズ 37, 2008) [初版第 6 刷発行, 2011].

[8] B. Alberts, A. Johnson, J. Lewis, M. Raff, K. Roberts, and P. Walter, *MOLECULAR BIOLOGY OF THE CELL, FOURTH EDITION*. (監訳: 中村桂子, 松原謙一, 『細胞の分子生物学 第 4 版』 (ニュートンプレス, 2004) [第 4 刷, 2007]).

[9] B. Alberts, D. Bray, K. Hopkin, A. Johnson, J. Lewis, M. Raff, K. Roberts, and P. Walter, *Essential Cell Biology, Second Edition*. (監訳: 中村桂子, 松原謙一, 『Essential 細胞生物学 (原書第 2 版)』 (南江堂, 2005) [第 3 刷発行, 2007]).

[10] K. Nishinari, Y. Okada, A. Schadschneider, and D. Chowdhury, Phys. Rev. Lett. **95**, 118101 (2005).

[11] N. Hirokawa, S. Niwa, and Y. Tanaka, Neuron **68**, 610 (2010).

[12] A. Parmeggiani, T. Franosch, and E. Frey, Phys. Rev. Lett. **90**, 086601 (2003).

[13] M. R. Evans, R. Juhász, and L. Santen, Phys. Rev. E **68**, 026117 (2003).

[14] W. Knospe, L. Santen, A. Schadschneider, and M. Schreckenberg, J. Phys. A: Math. Gen. **35**, 3369 (2002).

[15] G. F. Gu, W. Chen, and W. X. Zhou, Physica A **387**, 3173 (2008).

[16] 増川純一, 水野貴之, 村井浄信, 尹 熙元, 『株価の経済物理学』 (培風館, 2011).

[17] M. D. Gould, M. A. Porter, S. Williams, M. McDonald, D. J. Fenn, and S. D. Howison, Quant. Finance **13**, 1709 (2013).

[18] H. Luckock, Quant. Finance **3**, 385 (2003).

[19] R. N. Mantegna and H. E. Stanley, *An Introduction to Econophysics: Correlations and Complexity in Finance* (Cambridge University Press, Cambridge, 2000). (訳: 中嶋眞澄, 『経済物理学入門: ファイナンスにおける相関と複雑性』 (エコノミスト社, 2000)).

[20] F. Slanina, Eur. Phys. J. B **61**, 225 (2008).

[21] T. M. Liggett, *Interacting Particle Systems* (Springer-Verlag, New York, 1985).

[22] C. T. MacDonald, J. H. Gibbs, and A. C. Pipkin, Biopolymers **6**, 1 (1968).

[23] B. Derrida, M. R. Evans, V. Hakim, and V. Pasquier, J. Phys. A: Math. Gen. **26**, 1493 (1993).

[24] A. B. Kolomeisky, G. M. Schütz, E. B. Kolomeisky, and J. P. Straley, J. Phys. A: Math. Gen. **31**, 6911 (1998).

[25] T. Sasamoto, J. Phys. A: Math. Gen. **32**, 7109 (1999).

[26] R. A. Blythe and M. R. Evans, J. Phys. A: Math. Theor. **40**, R333 (2007).

[27] J. Krug, Phys. Rev. Lett. **67**, 1882 (1991).

[28] T. Sasamoto, S. Mori, and M. Wadati, J. Phys. Soc. Jpn. **65**, 2000 (1996).

[29] D. Chowdhury, L. Santen, and A. Schadschneider, Phys. Rep. **329**, 199 (2000).

[30] D. Yanagisawa, A. Tomoeda, R. Jiang, and K. Nishinari, JSIAM Letters **2**, 61 (2010).

[31] D. Yanagisawa, Y. Suma, A. Tomoeda, A. Miura, K. Ohtsuka, and K. Nishinari, Transportation Research Part C **37**, 238 (2013).

[32] T. Ezaki and K. Nishinari, J. Phys. A: Math. Theor. **45**, 185002 (2012).

[33] S. Ichiki, J. Sato, and K. Nishinari, Eur. Phys. J. B **89**, 135 (2016).

[34] S. Ichiki, J. Sato, and K. Nishinari, J. Phys. Soc. Jpn. **85**, 044001 (2016).

[35] S. Ichiki and K. Nishinari, Physica A **420**, 304 (2015).

[36] S. Ichiki and K. Nishinari, *Proceedings of the International Conference on Social Modeling and Simulation, plus Econophysics Colloquium 2014* (Springer International Publishing, Springer Proceedings in Complexity, 2015) p. 75.

[37] A. Parmeggiani, T. Franosch, and E. Frey, Phys. Rev. E **70**, 046101 (2004).

[38] T. Mitsudo and H. Hayakawa, J. Phys. A: Math. Gen. **39**, 15073 (2006).

[39] C. Arita, J. Phys. A: Math. Theor. **41**, 335001 (2008).

[40] S. Chandel, A. Chaudhuri, and S. Muhuri, Europhys. Lett. **110**, 18002 (2015).

[41] S. Katz, J. L. Lebowitz, and H. Spohn, J. Stat. Phys. **34**, 497, (1984).

[42] J. S. Hager, J. Krug, V. Popkov, and G. M. Schutz, Phys. Rev. E **63**, 056110 (2001).

[43] H. D. Vuijk, R. Rens, M. Vahabi, F. C. MacKintosh, and A. Sharma, Phys. Rev. E **91**, 032143 (2015).

[44] P. Greulich and A. Schadschneider, Phys. Rev. E **79**, 031107 (2009).

[45] S. Muhuri, Europhys. Lett. **101**, 38001 (2013).

[46] I. Dhiman and A. K. Gupta, Europhys. Lett. **107**, 20007 (2014).

[47] I. Neri, N. Kern, and A. Parmeggiani, Phys. Rev. Lett. **110**, 098102 (2013).

[48] I. Neri, N. Kern, and A. Parmeggiani, New J. Phys. **15**, 085005 (2013).

[49] T. Masuda, K. Nishinari, and A. Schadschneider, Phys. Rev. Lett. **112**, 138701 (2014).

[50] B. Derrida, E. Domany, and D. Mukamel, J. Stat. Phys. **69**, 669 (1992).

[51] M. J. Lighthill and G. B. Whitham, Proc. R. Soc. London, Ser. A **229**, 281 (1955).

[52] M. J. Lighthill and G. B. Whitham, Proc. R. Soc. London, Ser. A **229**, 317 (1955).

[53] J. Sato and K. Nishinari, Phys. Rev. E **93**, 042113 (2016).

[54] P. Bak, M. Paczuski, and M. Shubik, Physica A **246**, 430 (1997).

[55] S. Maslov, Physica A **278**, 571 (2000).

[56] D. Challet and R. Stinchcombe, Physica A **300**, 285 (2001).

[57] R. D. Willmann, G. M. Schütz, and D. Challet, Physica A **316**, 430 (2002).

[58] T. Preis, S. Golke, W. Paul, and J. J. Schneider, Europhys. Lett. **75**, 510 (2006).

[59] T. Preis, S. Golke, W. Paul, and J. J. Schneider, Phys. Rev. E **76**, 016108 (2007).

[60] J. Maskawa, Physica A **382**, 172 (2007).

[61] R. N. Mantegna and H. E. Stanley, Nature **376**, 46 (1995).

[62] P. Gopikrishnan, M. Meyer, L. A. N. Amaral, and H. E. Stanley, Eur. Phys. J. B **3**, 139 (1998).

[63] V. Plerou, P. Gopikrishnan, L. A. N. Amaral, M. Meyer, and H. E. Stanley, Phys. Rev. E **60**, 6519 (1999).

[64] 高安秀樹, 高安美佐子,『エコノフィジックス: 市場に潜む物理法則』(日本経済新聞社, 2001).

[65] Y. Hashimoto, T. Ito, T. Ohnishi, M. Takayasu, H. Takayasu, and T. Watanabe, Quant. Finance **12**, 893 (2012).

[66] 井庭崇, 福原義久,『複雑系入門: 知のフロンティアへの冒険』(NTT 出版, 1998) [初版第 19 刷発行, 2013].

[67] 高安秀樹, 高安美佐子,『経済・情報・生命の臨界ゆらぎ: 複雑系科学で近未来を読む』(ダイヤモンド社, 2000).

[68] N. Johnson, *Simply Complexity: A Clear Guide to Complexity Theory* (Oneworld Publications, London, 2007). (訳: 坂本芳久,『複雑で単純な世界: 不確実なできごとを複雑系で予測する』(インターシフト, 2011) [第 2 刷発行, 2013]).

[69] 東京証券取引所 [編],『入門 日本の証券市場』(東洋経済新報社, 2004).

[70] R. Cont, Quant. Finance **1**, 223 (2001).

[71] G. Harras and D. Sornette, Swiss Finance Institute Research Paper Series No. 08-16, 1-37 (2008).

[72] H. Takayasu, H. Miura, T. Hirabayashi, and K. Hamada, Physica A **184**, 127 (1992).

[73] K. Yamada, H. Takayasu, T. Ito, and M. Takayasu, Phys. Rev. E **79**, 051120 (2009).

[74] A. Johansen and D. Sornette, Eur. Phys. J. B **17**, 319 (2000).

[75] D. Sornette, *Why Stock Market Crash: Critical Events in Complex Financial Systems* (Princeton University Press, Princeton, 2003). (監訳: 森谷博之,『[入門] 経済物理学: 暴落はなぜ起こるのか？』(PHP 研究所, 2004)).

[76] Y. Malevergne, V. Pisarenko, and D. Sornette, Swiss Finance Institute Research Paper Series No. 09-40, 1-9 (2009).

[77] 青山秀明, 家富洋, 池田裕一, 相馬亘, 藤原義久,『経済物理学: Econophysics』(共立出版, 2008) [初版 3 刷発行, 2010].

Acknowledgments

I would like to express the deepest appreciation to my adviser Prof. Katsuhiro Nishinari, who has given insightful comments and encouragement. I would also like to thank my dissertation committee members: Prof. Naomichi Hatano, Prof. Kiyoshi Kotani, Prof. Ralph Willox and Prof. Daichi Yanagisawa (alphabetical order) for their valuable feedback on this dissertation.

I wish to thank past and present all stuffs, students and academics of Nishinari laboratory. In particular, I gratefully acknowledge Prof. Jun Sato for invaluable comments and advices through collaborative research. Prof. Daichi Yanagisawa and Dr. Takahiro Ezaki offered helpful comments on my studies. I am genuinely thankful to them. I am grateful to Kohei Kikuchi for kindly cooperation on check of the sentence in this dissertation.

I have been blessed with excellent friends and colleagues. In particular, Kakeru Rai gave me valuable knowledge on programmings. I received helpful suggestions with respect to English from Ayla Wagatsuma. Dr. Hiroko Watanabe told me teaching in response to some consultations as a researcher. I take this opportunity to express my appreciation to them.

I would like to express my gratitude to Iue Memorial Foundation for their financial support. I also thank Japan Exchange Group, Inc. for giving me the opportunity to study in doctoral course.

Finally, I would like to thank my family and Hana Shibuya for everything in my daily life.

June 2016
Shingo Ichiki